frontiers in Earth Science

ORIGINAL RESEARCH
published: 05 February 2021
doi: 10.3389/feart.2020.596178

Carbon Isotope Chemostratigraphy Across the Permian-Triassic Boundary at Chaotian, China: Implications for the Global Methane Cycle in the Aftermath of the Extinction

Masafumi Saitoh[1,2,3]* *and Yukio Isozaki*[4]

[1]*Institut des Sciences de la Terre, Université de Lausanne, Lausanne, Switzerland,* [2]*Research and Development (R&D) Center for Submarine Resources, Japan Agency for Marine-Earth Science and Technology (JAMSTEC), Yokosuka, Japan,* [3]*Earth-Life Science Institute, Tokyo Institute of Technology, Tokyo, Japan,* [4]*Department of Earth Science and Astronomy, The University of Tokyo, Tokyo, Japan*

OPEN ACCESS

Edited by:
David Mark Hodgson, University of Leeds, United Kingdom

Reviewed by:
Genming Luo, China University of Geosciences Wuhan, China
Mike Rogerson, University of Hull, United Kingdom

***Correspondence:**
Masafumi Saitoh
saitoh.m.ab@gmail.com

Specialty section:
This article was submitted to Sedimentology, Stratigraphy and Diagenesis, a section of the journal Frontiers in Earth Science

Received: *19 August 2020*
Accepted: *01 December 2020*
Published: *05 February 2021*

Citation:
Saitoh M and Isozaki Y (2021) Carbon Isotope Chemostratigraphy Across the Permian-Triassic Boundary at Chaotian, China: Implications for the Global Methane Cycle in the Aftermath of the Extinction. Front. Earth Sci. 8:596178. doi: 10.3389/feart.2020.596178

During the end-Permian extinction, a substantial amount of methane (CH_4) was likely released into the ocean-atmosphere system associated with the Siberian Traps volcanism, although fluctuations in the global CH_4 cycle in the aftermath of the extinction remain poorly understood. The carbon (C) isotopic composition of carbonate ($\delta^{13}C_{carb}$) across the Permian-Triassic boundary (P-TB) was analyzed at Chaotian, South China. The $\delta^{13}C_{carb}$ values decrease from ca. +1 to –2‰ across the P-TB, possibly caused by a collapse of primary productivity associated with the shallow-marine extinction. The frequent intercalation of felsic tuff layers around the P-TB suggests that a volcanogenic carbon dioxide (CO_2) input to the surface oceans may also have contributed to the $\delta^{13}C_{carb}$ decline. The magnitude of the $\delta^{13}C_{carb}$ decrease (~3‰) is substantially smaller than the magnitude of a decrease in C isotopic composition of organic matter ($\delta^{13}C_{org}$) in the same P-TB interval (~7‰). This apparent $\delta^{13}C_{carb}$-$\delta^{13}C_{org}$ decoupling could be explained by proliferation of methanogen ("methanogenic burst") in the sediments. A global $\delta^{13}C$ compilation shows a large variation in marine $\delta^{13}C_{org}$ records, implying that the "methanogenic burst" according to the Siberian Traps volcanism may have contributed, at least in part, to the $\delta^{13}C_{org}$ variability and to the elevated CH_4 levels in the atmosphere. The present and previous observations allow us to infer that the global CH_4 cycle may have fluctuated substantially in the aftermath of the extinction.

Keywords: end-Permian extinction, global CH_4 cycle, methanogenesis, methanotrophy, anaerobic oxidation of methane (AOM), global warming, variable $\delta^{13}C_{org}$ records

INTRODUCTION

The end-Permian extinction was one of the largest biodiversity crises in the Phanerozoic (e.g., Erwin, 2006; Alroy, 2010; Shen et al., 2011a; Stanley, 2016), and many geologic events around the Permian-Triassic boundary (P-TB) have been proposed as the cause of the extinction, including a bolide impact (e.g., Xu et al., 1985; Becker et al., 2004), Siberian Traps volcanism (e.g., Renne and Basu, 1991; Campbell et al., 1992; Kamo et al., 2003; Reichow et al., 2009; Burgess and Bowring, 2015) and the associated massive release of thermogenic gases (e.g., Wignall, 2001; Retallack and Jahren, 2008; Svensen et al., 2009; Shen et al., 2012; Polozov et al., 2016) and resulting global warming (e.g., Hallam and Wignall, 1997; Kidder and Worsley, 2004; Brand et al., 2012; Joachimski et al., 2012), oceanic anoxia (e.g., Wignall and Hallam, 1992; Wignall and Twitchett, 1996; Isozaki, 1997; Algeo et al., 2008; Shen et al., 2011c; Schobben et al., 2015) accompanied by H_2S poisoning (e.g., Grice et al., 2005; Kump et al., 2005; Zhang et al., 2017; Zhou et al., 2017) and hypercapnia (Knoll et al., 1996, 2007), and oceanic acidification (e.g., Heydari et al., 2003; Payne et al., 2007; Clapham and Payne, 2011; Clarkson et al., 2015; Baresel et al., 2017; Garbelli et al., 2017; Jurikova et al., 2020). However, the ultimate trigger mechanisms of the extinction remain a topic of discussion (e.g., Payne and Clapham, 2012; Isozaki, 2019; Racki, 2020).

The global carbon (C) cycle was likely perturbed during the Permian-Triassic transition in association with those geologic events that potentially contributed to the extinction (e.g., Kump and Arthur, 1999). Stable C isotope geochemistry is useful to correlate sections in different regions and to reveal the changes in the global C cycle (e.g., Hayes et al., 1999). Plenty of studies analyzed the C isotopic composition of carbonate ($\delta^{13}C_{carb}$) of P-TB rocks and documented a negative $\delta^{13}C_{carb}$ shift by ~5‰ during the extinction in various sections around the world, including South China, Iran, Armenia, northern Italy, Austria, Slovenia, and Pakistan (e.g., Magaritz et al., 1988; Baud et al., 1989; Holser et al., 1989; Jin et al., 2000; Richoz, 2006; Horacek et al., 2007a; Horacek et al., 2007b; Korte and Kozur, 2010 and references therein; Shen et al., 2013; Schobben et al., 2016; Joachimski et al., 2020). Although several studies pointed out a substantial diagenetic overprint and/or erosional unconformity on the P-TB $\delta^{13}C_{carb}$ records (e.g., Heydari et al., 2001; Heydari and Hassanzadeh, 2003; Grasby and Beauchamp, 2008; Yin et al., 2014; Schobben et al., 2016; Li and Jones, 2017), the widely recognized P-TB $\delta^{13}C_{carb}$ decrease has been generally regarded as an original isotopic signal of seawater (Bagherpour et al., 2019).

Considering a simple box model of the surface-ocean C pool, two principle mechanisms could explain the P-TB $\delta^{13}C$ decrease in marine carbonates: 1) a decrease in the output and 2) an increase in the input of ^{13}C-depleted C (e.g., Korte and Kozur, 2010). A collapse in primary productivity and reduction in biological pump ("strangelove oceans") corresponds to the former mechanism (e.g., Kump, 1991), although it may have produced only a ~3‰ negative $\delta^{13}C_{carb}$ shift (Rampino and Caldeira, 2005) and might not be sufficient to explain larger P-TB $\delta^{13}C$ declines commonly observed around the world. The increase in the input of ^{13}C-depleted C to the surface oceans seems to be more important (e.g., Payne and Clapham, 2012), and several geologic events have been proposed for the C injection, including volcanogenic CO_2 emission involved in the Siberian Traps volcanism (e.g. Renne et al., 1995; Hansen, 2006), methane (CH_4) release during destabilization of submarine and permafrost clathrates or thermal alteration of coal by volcanic intrusion (e.g. Erwin, 1993; Morante, 1996; Krull and Retallack, 2000; Berner, 2002; Sarkar et al., 2003; Retallack and Jahren, 2008), enhanced erosion and reoxidation of sedimentary organic matter or terrestrial soil (e.g. Baud et al., 1989; Holser et al., 1989; Ward et al., 2000; Sephton et al., 2005), and the oceanic overturn or shoaling of deep-water (e.g., Kajiwara et al., 1994; Knoll et al., 1996; Algeo et al., 2007a). Korte and Kozur (2010) comprehensively correlated the P-TB $\delta^{13}C_{carb}$ records of shelf carbonates on a global scale. Based on a gradually decreasing trend toward the P-TB, the authors suggested that the $\delta^{13}C_{carb}$ decrease was caused by a combination of the Siberian Traps volcanism and a shoaling of anoxic deep-waters onto shelves.

A negative shift of the C isotopic composition of organic C ($\delta^{13}C_{org}$) across the P-TB has been reported in marine strata in many sections such as Arctic Canada (e.g., Grasby and Beauchamp, 2008; Algeo et al., 2012), Greenland (e.g., Twitchett et al., 2001), Spitsbergen (e.g., Wignall et al., 1998; Zuchuat et al., 2020), South China (e.g., Cao et al., 2002), Japan (e.g., Takahashi et al., 2010), and Australia (e.g., Morante, 1996). The marine $\delta^{13}C_{org}$ decrease has been correlated normally with the negative $\delta^{13}C_{carb}$ shift in shelf carbonates by assuming that the $\delta^{13}C_{carb}$ and $\delta^{13}C_{org}$ trends were parallel and the difference between the $\delta^{13}C_{carb}$ and $\delta^{13}C_{carb}$ values ($\Delta^{13}C$) was consistent during the Permian-Triassic transition, although the $\Delta^{13}C$ value is generally controlled by several factors such as carbon dioxide (CO_2)-fixing enzymes and atmospheric CO_2 levels (pCO_2) (e.g., Hayes et al., 1999). A parallel $\delta^{13}C_{carb}$ and $\delta^{13}C_{org}$ decline has been reported in the P-TB intervals in Austria (Magaritz et al., 1992), Italy (Sephton et al., 2002), mid-Panthalassa (Musashi et al., 2001), and Kashmir (Algeo et al., 2007b). However, some studies pointed out a $\delta^{13}C_{carb}$-$\delta^{13}C_{org}$ decoupling across the P-TB. The $\Delta^{13}C$ values apparently decrease in some sections in South China, Slovenia, and Iran (Riccardi et al., 2007), and increase in some other Chinese sections (e.g., Shen et al., 2012).

The $\delta^{13}C_{org}$ decrease in a terrestrial P-TB succession has also been reported in South China (e.g., Shen et al., 2011a), South Africa (e.g., Ward et al., 2005; Gastaldo et al., 2020), Antarctica (e.g., Krull and Retallack, 2000), Australia (Morante, 1996), Madagascar (de Wit et al., 2002), and Germany (Scholze et al., 2017). However, the apparent $\delta^{13}C_{org}$ trends on land are generally variable compared to those of marine sediments, and the P-TB $\delta^{13}C_{org}$ decline is not clearly recognized in many terrestrial sections (e.g., Retallack et al., 2005; Fielding et al., 2019). Moreover, the P-TB is generally not well assigned in the terrestrial successions due to their poorer biostratigraphic constraints. Under these circumstances, it is still difficult to correlate the terrestrial $\delta^{13}C_{org}$ records well with the marine $\delta^{13}C_{org}$ and $\delta^{13}C_{carb}$ records.

Previous studies particularly suggested that a substantial amount of CH_4 was released into the ocean/atmosphere during the Siberian Traps volcanism via several processes, including volcanic intrusion into coal (e.g., Retallack and Jahren, 2008; Shen et al., 2012; Rampino et al., 2017), destabilization of submarine and permafrost clathrates (e.g.,

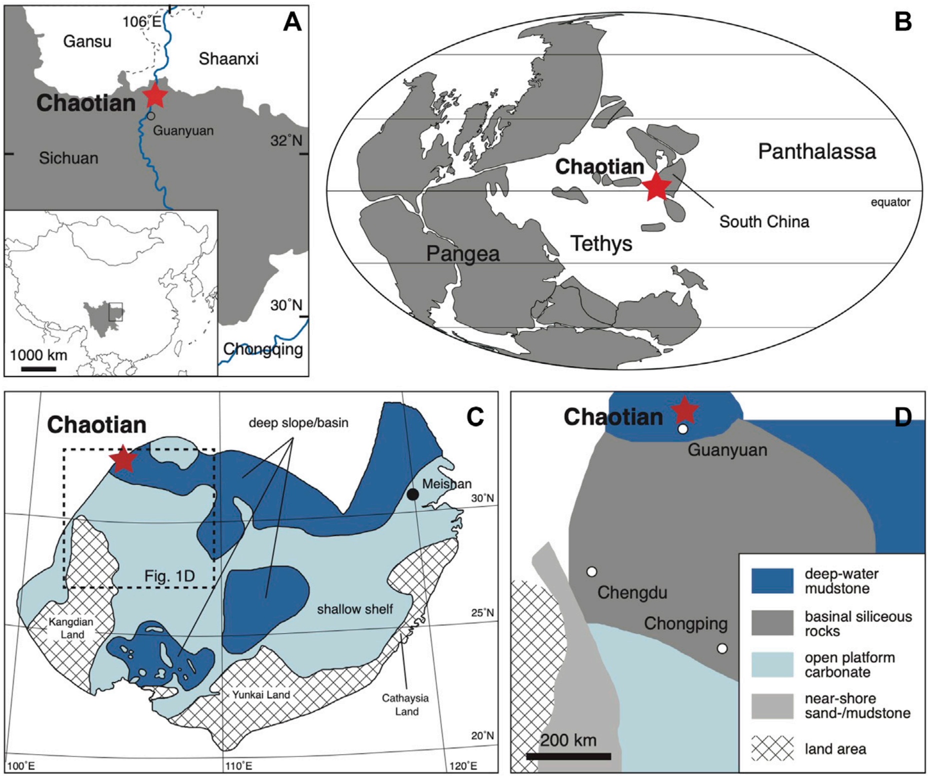

FIGURE 1 | Locality and paleogeographic maps of Chaotian. **(A)** Location map of Chaotian. **(B)** Global paleogeographic map around the P-TB (modified from Muttoni et al., 2009). **(C)** Sedimentary facies distribution in South China in the late Changhsingian (late Late Permian) (modified from Wang and Jin, 2000). **(D)** Detailed sedimentary facies in the square in C (modified from Zhu et al., 1999).

Krull et al., 2000; Krull et al., 2004; Brand et al., 2016), and enhanced microbial methanogenesis ("methanogenic burst") (Rothman et al., 2014). As CH_4 is a potent greenhouse gas, the huge CH_4 input may have contributed to climate warming in the aftermath of the extinction (e.g., Hallam and Wignall, 1997; Joachimski et al., 2012; Sun et al., 2012; Cui and Kump, 2015). However, the global CH_4 cycle during the Permian-Triassic transition has been poorly examined and constrained. In this study, we analyzed the $\delta^{13}C_{carb}$ records of the P-TB carbonates at Chaotian in northern Sichuan, South China. Together with the previously reported $\delta^{13}C_{org}$ records of the same interval, we examined the sedimentary C cycle in eastern Paleotethys during the Permian-Triassic transition. Moreover, we compiled the $\delta^{13}C_{carb}$ and $\delta^{13}C_{org}$ records of P-TB successions in various marine and terrestrial environments around the world, to examine whether the isotopic signal detected at Chaotian was a global one. Based on those results, we suggest fluctuations in the global CH_4 cycle in the aftermath of the end-Permian extinction.

GEOLOGICAL SETTING AND STRATIGRAPHY

During the Permian to early Triassic, South China was isolated from other continental blocks and located at low latitudes on the eastern side of Pangea (**Figure 1B**; Muttoni et al., 2009). Shallow-marine carbonates and terrigenous clastics with diverse fossils accumulated extensively on its platform (e.g., Zhao et al., 1981; Yang et al., 1987; Jin et al., 1998). In northern Sichuan along the northwestern edge of South China, carbonates and mudstones of deep-water facies accumulated on a slope/basin that faced on the eastern Paleotethys (**Figure 1C**; Zhu et al., 1999; Wang and Jin, 2000). The Chaotian section is located ca. 20 km to the north of Guangyuan city in northern Sichuan (**Figure 1**; 32°37′N, 105°51′E; Isozaki et al. 2004). At Chaotian, Guadalupian (middle Permian) to lowermost Triassic carbonates are continuously exposed along the bank of the Jialingjiang River in a narrow gorge called Mingyuexia. We mapped the eastern bank of the gorge on the southern limb of an E-W trending anticline.

The Permo-Triassic rocks at Chaotian (>300 m thick in total) are composed of the Guadalupian Maokou Formation, the Lopingian Wujiaping and Dalong formations, and the lowermost Triassic Feixianguan Formation, in ascending order (**Figure 2**; Isozaki et al., 2004; Isozaki et al., 2007; Saitoh et al., 2013a; Saitoh et al., 2013b; Saitoh et al., 2014a). The Maokou Formation (>150 m thick) is composed mainly of massive dark gray bioclastic limestone with diverse shallow-marine fossils, such as calcareous algae, brachiopods, ostracodes, crinoids, rugosa corals, and fusulines. However, the uppermost part

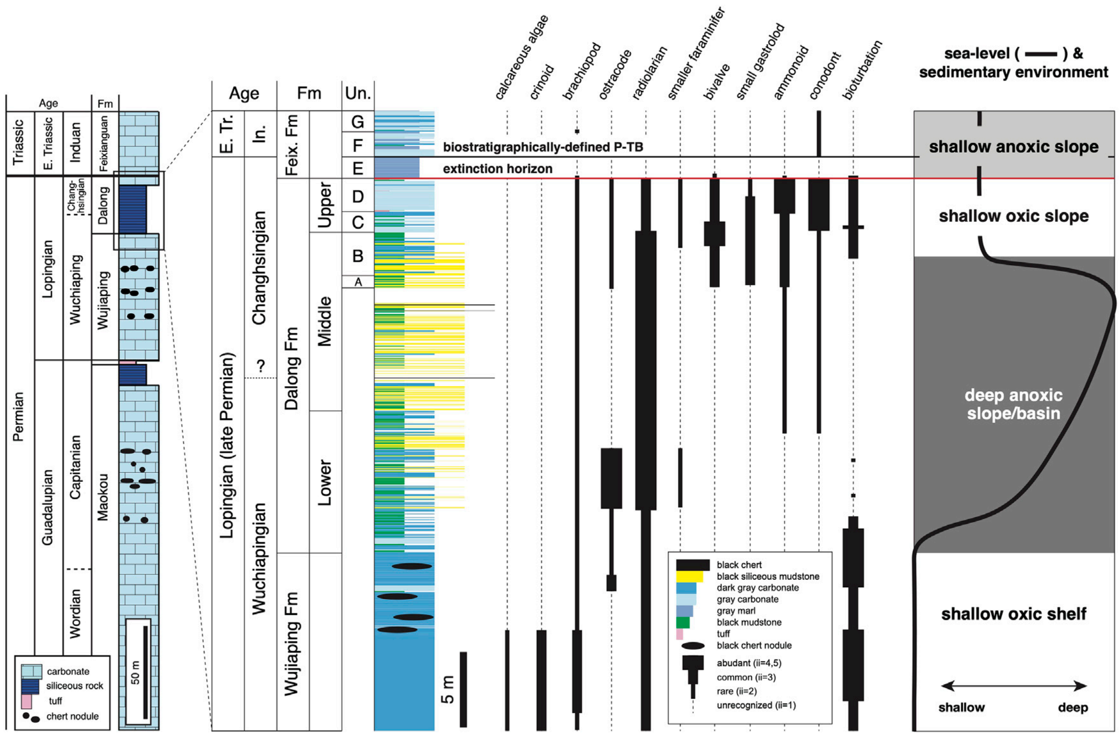

FIGURE 2 | The analyzed P-TB interval at Chaotian with ranges of fossil groups (modified from Saitoh et al., 2014a). Un.: unit in Isozaki et al. (2007), E. Tr.: Early Triassic, In.: Induan, Feix.: Feixianguan, ii: ichnofabric index.

(~11 m thick) of the Maokou Formation is composed of thinly bedded black calcareous mudstone and black chert/siliceous mudstone with abundant radiolarians, conodonts, and ammonoids. The Wujiaping Formation (~70 m thick) is composed mainly of massive dark gray bioclastic limestone with black chert nodules/lenses, containing shallow-marine fossils such as fusulines, smaller foraminifer, rugosa corals, calcareous algae and brachiopods. At the base of the Wujiaping Formation, a ca. 2 m thick tuffaceous Wangpo bed occurs. The Dalong Formation (~25 m thick) is composed mainly of thinly bedded black mudstone, black siliceous mudstone and dark gray limestone with radiolarians, ammonoids, bivalves, and brachiopods. The Feixianguan Formation (>30 m thick) is composed mainly of thinly bedded light gray micritic limestone containing few conodonts, ammonoids, and brachiopods.

Zhao et al. (1978) and Yang et al. (1987) originally described the overall biostratigraphy of the Chaotian section based on fusulines, conodonts, and ammonoids. Isozaki et al. (2004) and Isozaki et al. (2007) re-examined the stratigraphy of the section that spans across the two mass extinction intervals; i.e. the Guadalupian-Lopingian boundary (G-LB) and the P-TB in higher resolution. More analyses on the litho-, bio-, and chemo-stratigraphy of the Chaotian section added further information (Isozaki et al., 2008; Lai et al., 2008; Saitoh et al., 2013a; Saitoh et al., 2013b; Jost et al., 2014; Saitoh et al., 2014b; Saitoh et al., 2015; Saitoh et al., 2017). Isozaki et al. (2007) and Ji et al. (2007) constructed the detailed lithostratigraphy and conodont zonation for the ~12 m thick interval across the P-TB, and suggested that intermittent felsic volcanism may have contributed to the extinction. Cao et al. (2010) analyzed the $\delta^{13}C_{carb}$ values around the P-TB and found a negative $\delta^{13}C$ excursion around the extinction horizon. Saitoh et al. (2014a) analyzed the nitrogen and organic C isotopic composition of the ~40 m thick P-TB interval at Chaotian and suggested enhanced nitrogen fixation in the anoxic oceans throughout the Changhsingian.

In the present study, we focused on the ~40 m thick P-TB interval at Chaotian (**Figure 2**). This interval is identical to that analyzed in Saitoh et al. (2014a), which contains the ~12 m thick carbonates analyzed in Isozaki et al. (2007). Fresh rock samples, collected from outcrops and from core samples by scientific drilling to a depth of >30 m, were prepared as polished slabs and thin sections for describing microtextures by petrographical observations. The analyzed P-TB interval is composed of three stratigraphic units: 1) the upper Wujiaping Formation, 2) the Dalong Formation, and 3) the lowermost Feixianguan Formation, in ascending order. The upper Wujiaping Formation (~10 m thick) is composed mainly of massive dark gray limestone (lime mudstone/wackestone) with some sandy/muddy limestones (**Figure 3D**). Black chert nodules (<10 cm in diameter) occur in the uppermost part of the Wujiaping Formation. The upper Wujiaping limestones contain diverse shallow-marine fossils such as calcareous algae, crinoids, brachiopods, radiolarians,

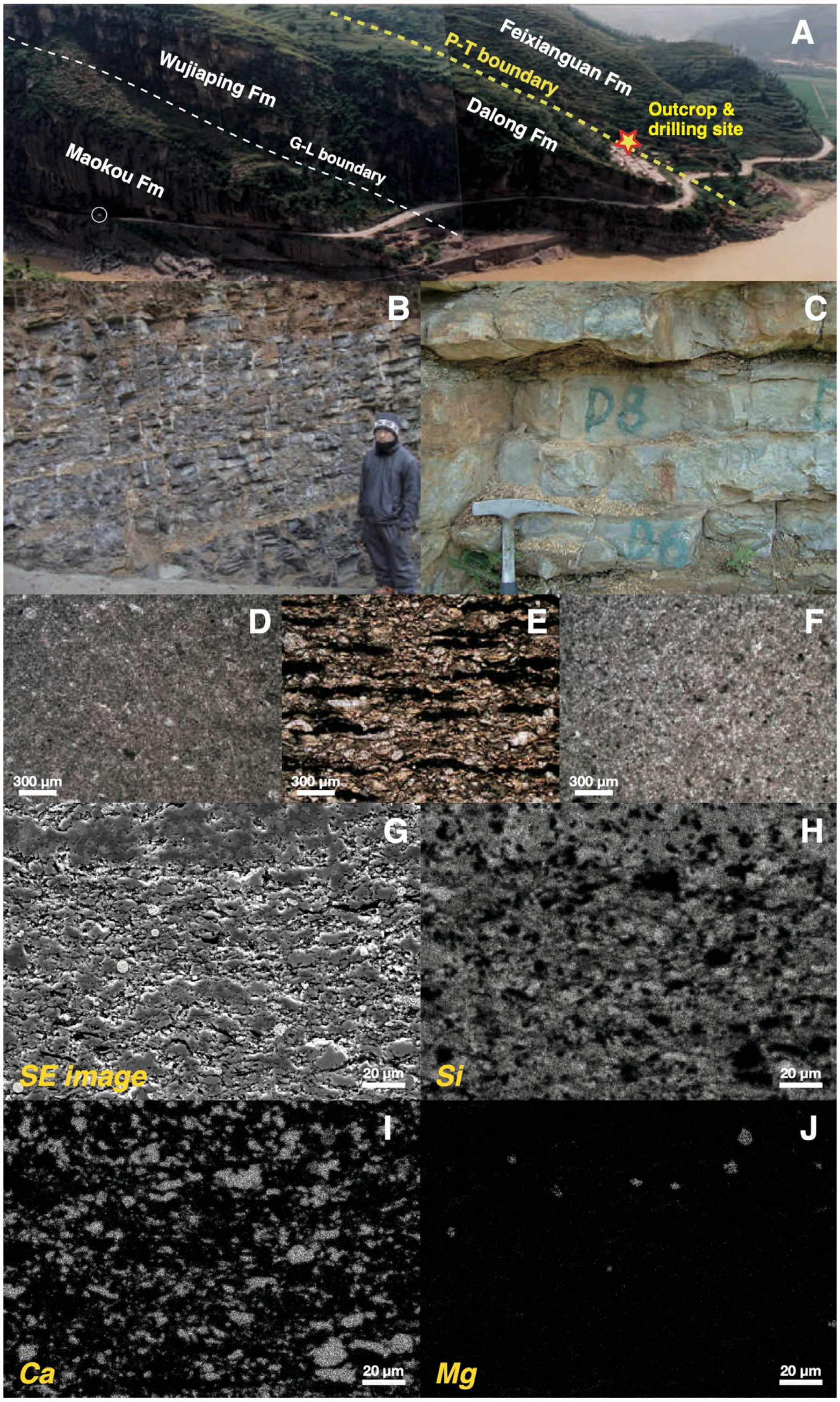

FIGURE 3 | A distant view and photographs of the P-TB interval at Chaotian. **(A)** A distant view of Chaotian (circled car for scale). **(B,C)** Outcrops of the uppermost Dalong limestones. **(D–F)** Thin sections of bioclastic limestone in the upper Wujiaping Formation **(D)**, calcareous mudstone in the Dalong Formation **(E)**, and lowermost Feixianguan limestone **(F)**. **(G-J)** Secondary electron (SE) image **(G)** and element maps **(H–J)** of calcareous mudstone in the Dalong Formation. Carbonates in the mudstones are mainly finely-fragmented bioclasts with few secondary dolomites.

and ostracodes. Burrows frequently occur in the upper Wujiaping limestones.

The Dalong Formation (~25 m thick) is composed mainly of thinly bedded black calcareous mudstone, black siliceous mudstone, dark gray muddy limestone, and bedded gray limestone (lime mudstone/wackestone) (**Figures 2**, **3**). The Dalong Formation contains abundant radiolarians with a minor amount of ostracodes, brachiopods, ammonoids, and conodonts, bivalves and small foraminifers. The uppermost (~3.5 m thick) part of the Dalong Formation mostly consists of bedded gray limestone (lime mudstone/wackestone) ('Unit C and D' in Isozaki et al., 2007). Thin (<10 cm thick) acidic tuff layers frequently occur in these limestones. Burrows are observed in the lower and upper Dalong Formation, although bioturbation is generally absent in the middle Dalong Formation. Small pyrite framboids (mostly 3–7 μm in diameter) occur abundantly throughout the Dalong Formation. The lowermost Feixianguan Formation (~5 m thick) is composed of thinly bedded gray marl and light gray micritic limestone with some sandy/muddy limestones. In particular, the lowermost (1.4 m thick) part ('Unit E' in Isozaki et al., 2007) is composed of gray marl. This marl unit is almost barren of fossil, although few ammonoids and bivalves occur from the basal part. The upper part of the lowermost Feixianguan Formation consists of light gray micritic limestone containing few conodonts and brachiopods. Few trace fossils are recognized in the lowermost Feixianguan Formation.

Based on index fossils (fusulines, conodonts, ammonoids, corals, and brachiopods), the analyzed P-TB interval at Chaotian is dated as follows (**Figure 2**; Zhao et al., 1978; Yang et al., 1987; Isozaki et al., 2004; Isozaki et al., 2007): The upper Wujiaping Formation is correlated with the Wuchiapingian (early Lopingian). The lower Dalong Formation is correlated with the late Wuchiapingian, whereas the middle Dalong Formation belongs to the late Wuchiapingian to early Changhsingian. The upper Dalong Formation is correlated with the late Changhsingian. The lowermost Feixianguan Formation is correlated with the latest Changhsingian to early Induan (early Early Triassic). The main extinction horizon is assigned at the base of the Feixianguan Formation ('Unit D/E boundary' in Isozaki et al., 2007), whereas the biostratigraphically defined P-TB is assigned at the base of the overlying micritic limestones ('Unit E/F boundary' in Isozaki et al., 2007). Based on the litho- and bio-facies, the sedimentary environments of the three stratigraphic units of the analyzed P-TB interval were reconstructed (**Figure 2**; Saitoh et al., 2014a). The upper Wujiaping limestones were deposited on the shallow euphotic shelf under oxic conditions. In contrast, the lower and middle Dalong Formation was deposited on the relatively deep slope/basin under anoxic conditions. The upper Dalong limestones were deposited on the relatively shallow slope below the storm wave base under oxic conditions. The lowermost Feixianguan formations were deposited on a relatively shallow slope under anoxic conditions.

ANALYTICAL METHODS

Fresh rock samples were carefully chosen based on detailed observations of polished slabs and thin sections. Powdered sample was reacted with 100% phosphoric acid at 28°C for 24 h using a GasBench (Thermo Fisher Scientific). The extracted CO_2 was separated in a chromatography line with a helium flow, and the carbon and oxygen isotope ratios were measured with a DELTA V PLUS mass spectrometer. The carbonate carbon and oxygen isotopic compositions are presented using the delta notation $\delta^{13}C = ((^{13}C/^{12}C)_{sample}/(^{13}C/^{12}C)_{standard}-1)$ and $\delta^{18}O = ((^{18}O/^{16}O)_{sample}/(^{18}O/^{16}O)_{standard}-1)$, respectively. The $\delta^{13}C$ and $\delta^{18}O$ values are reported in ‰ relative to the Vienna Peedee Belemnite (V-PDB) standard. The analytical reproducibility of the $\delta^{13}C_{carb}$ and $\delta^{18}O_{carb}$ values was better than 0.1 and 0.1‰, respectively.

RESULTS

Table 1 lists all the measured $\delta^{13}C_{carb}$ and $\delta^{18}O_{carb}$ values of the P-TB interval. **Figure 4** shows chemostratigraphic profiles of the $\delta^{13}C_{carb}$, $\delta^{18}O_{carb}$, $\delta^{13}C_{org}$, and $\Delta^{13}C$ values and TOC contents. The $\delta^{13}C_{org}$ values and TOC contents were previously reported in Saitoh et al. (2014a). **Figure 5** shows a $\delta^{13}C_{carb}$-$\delta^{18}O_{carb}$ cross plot. The $\delta^{13}C_{carb}$ values range from −6.9 to +4.3‰, with an average value of ca. 0‰. The $\delta^{18}O_{carb}$ values range from −7.9 to −2.9‰, with an average value of ca. −5.9‰.

The $\delta^{13}C_{carb}$ values are consistently ca. +4‰ in the upper Wujiaping Formation and decrease from ca. +4‰ to −2‰ across the Wujiaping/Dalong formation boundary. In the Dalong Formation, the $\delta^{13}C_{carb}$ values increase slightly from ca. −2 to +1‰ upward except for some anomalously low (<−3‰) values (open symbols in **Figure 4**). The $\delta^{13}C_{carb}$ values decrease from ca. +1‰ to −2‰ across the Dalong/Feixianguan formation boundary (i.e., the P-TB) and are consistent around −2‰ in the lowermost Feixianguan carbonates. The present $\delta^{13}C_{carb}$ results around the P-TB are generally identical to the results in Cao et al. (2010). The $\delta^{18}O_{carb}$ values are somewhat variable in in the upper Wujiaping limestones and are mainly around −7‰ in the overlying Dalong Formation. Above the P-TB, the $\delta^{18}O_{carb}$ values are mostly around −6‰ in the lowermost Feixianguan Formation. The $\Delta^{13}C$ values are mainly between 27 and 29‰ in the upper Wujiaping Formation and decrease slightly to ca. 26‰ in the Dalong Formation. The $\Delta^{13}C$ values increase to ca. 30‰ in the overlying lowermost Feixianguan carbonates.

No linear correlation is observed between the $\delta^{13}C_{carb}$ and $\delta^{18}O_{carb}$ values (**Figure 5**). It indicates that secondary overprinting on the Chaotian carbonates is not significant (Knauth and Kennedy, 2009). In the chemostratigraphic profile, however, some $\delta^{13}C_{carb}$ values in the Dalong Formation are anomalously low (<−3‰; open symbols in **Figure 4**) and these samples were likely affected at least partly by the secondary addition of ^{13}C-depleted C. Except for these anomalous values, the present $\delta^{13}C_{carb}$ results represent a smooth chemostratigraphic trend in the analyzed interval. This trend may record secular changes in the $\delta^{13}C$ value of dissolved inorganic carbon (DIC) in seawater ($\delta^{13}C_{DIC}$) in the Lopingian to earliest Triassic. Based on the C isotopic

TABLE 1 | C and O isotopic composition of the analyzed P-TB interval at Chaotian. The $\delta^{13}C_{org}$ values and TOC contents were reported in Saitoh et al. (2014a).

Formation	Sample ID	Lithology	Thickness (m)	$\delta^{13}C_{carb}$ vs. VPDB (‰)	$\delta^{18}O_{carb}$ vs. VPDB (‰)	$\delta^{13}C_{org}$ vs. VPDB (‰)	$\Delta^{13}C$ vs. VPDB (‰)	TOC (%)
Feixianguan	G8	dark gray limestone	38.3	−1.7	−5.5	−29.6	27.9	0.0
Feixianguan	G6	dark gray limestone	38.0	−1.9	−6.1	−31.3	29.5	0.0
Feixianguan	G4	gray limestone	37.7	−1.8	−5.9	−31.4	29.7	0.1
Feixianguan	G1	dark gray limestone	37.3	−1.7	−5.7	−31.8	30.0	0.1
Feixianguan	F11	gray limestone	36.8	−1.8	−5.9	−31.6	29.9	0.1
Feixianguan	F7	dark gray limestone	36.5	−1.9	−4.9	−31.7	29.8	0.1
Feixianguan	F5	gray marl	36.3	−1.6	−5.5	−28.2	26.7	0.0
Feixianguan	F3	gray limestone	36.0	−1.3	−6.0	−30.8	29.5	0.0
Feixianguan	F1	gray limestone	35.7	−0.9	−6.9	−30.1	29.2	0.1
Feixianguan	E11	gray marl	35.1	−0.4	−5.8			
Feixianguan	E7	gray marl	34.8	−0.1	−4.4	−25.6	25.5	0.1
Feixianguan	E2	gray marl	34.4	0.1	−4.4	−25.0	25.0	0.1
Dalong	D19	gray limestone	33.7	1.0	−5.7	−28.2	29.2	0.0
Dalong	D15	gray limestone	33.3	0.4	−7.0	−25.6	26.0	0.1
Dalong	D13	gray limestone	33.1	−1.3	−7.5	−25.2	23.8	0.2
Dalong	D9	gray limestone	32.8	0.6	−5.7	−25.2	25.8	0.1
Dalong	D3	gray limestone	32.2	1.9	−4.0	−25.7	27.6	0.0
Dalong	C8	black mudstone	31.6	0.6	−7.0	−26.0	26.6	0.9
Dalong	C6	black mudstone	31.2	−0.2	−7.2	−26.7	26.4	2.0
Dalong	B33	black mudstone	30.3	0.2	−7.1	−27.1	27.3	1.6
Dalong	B26	black mudstone	29.7	0.3	−7.1	−27.2	27.4	1.5
Dalong	B20	dark gray muddy limestone	29.2	0.7	−6.7	−26.0	26.7	0.7
Dalong	B10	dark gray muddy limestone	28.5	−3.4	−6.0	−27.2	23.8	0.7
Dalong	B3	dark gray muddy limestone	28.0	−5.9	−6.0	−26.5	20.6	0.7
Dalong	A11	black mudstone	27.4			−26.6		4.8
Dalong	Dalong49	black mudstone	25.5	−2.6	−7.1	−26.8	24.2	10.1
Dalong	Dalong48	black mudstone	25.1	−0.4	−7.2	−26.8	26.4	10.4
Dalong	Dalong47	black mudstone	24.6	−2.1	−7.1	−26.6	24.6	10.0
Dalong	Dalong46	black mudstone	24.0	−4.1	−4.7	−26.7	22.7	8.1
Dalong	Dalong45	black mudstone	23.1	0.4	−6.6	−26.6	26.9	10.0
Dalong	Dalong44	black mudstone	22.9	0.6	−6.9	−26.8	27.3	9.9
Dalong	Dalong43	black mudstone	22.4	−0.5	−7.0	−26.7	26.1	12.3
Dalong	Dalong42	black mudstone	21.9	0.4	−6.9	−26.2	26.7	9.0
Dalong	Dalong41	black mudstone	20.3	−3.2	−5.0	−27.2	24.0	7.5
Dalong	Dalong40	black mudstone	20.0	−3.6	−5.3	−27.2	23.6	9.2
Dalong	Dalong39	black mudstone	19.8	−1.1	−7.8	−27.1	25.9	13.2
Dalong	Dalong38	black mudstone	19.3	−1.4	−7.2	−27.0	25.6	9.4
Dalong	Dalong37	black mudstone	19.0	−0.2	−7.2	−27.1	26.9	8.7
Dalong	Dalong36	black mudstone	18.5	−1.6	−6.0	−27.3	25.7	12.3
Dalong	Dalong34	black mudstone	18.2	−0.7	−7.0	−27.0	26.3	9.4
Dalong	Dalong33	black mudstone	17.9	−1.4	−7.3	−27.3	25.9	11.3
Dalong	Dalong31	black mudstone	17.7	−0.4	−7.4	−27.6	27.2	5.9
Dalong	Dalong30	dark gray muddy limestone	17.6	−6.9	−2.9	−28.5	21.6	2.5
Dalong	Dalong29	black mudstone	17.2	−1.6	−7.1	−27.2	25.6	10.0
Dalong	Dalong28	black mudstone	16.6	−2.3	−7.5	−27.2	25.0	3.9
Dalong	Dalong27	black mudstone	16.3	−1.8	−7.0	−27.4	25.6	8.3
Dalong	Dalong26	dark gray muddy limestone	16.1	−5.8	−4.7	−27.6	21.8	1.4
Dalong	Dalong25	dark gray muddy limestone	15.6	−1.9	−6.5	−27.3	25.3	5.8
Dalong	Dalong23	black mudstone	15.5	−2.3	−6.9	−26.8	24.5	15.1
Dalong	Dalong21	black mudstone	15.2	−1.3	−7.5	−27.1	25.8	10.3
Dalong	Dalong20	black mudstone	14.8	−1.6	−6.9	−27.4	25.8	11.9
Dalong	Dalong18	black mudstone	14.3	−0.5	−7.9	−27.0	26.5	12.4
Dalong	Dalong17	black mudstone	14.0	−0.6	−7.2	−27.2	26.6	11.6
Dalong	Dalong14	dark gray muddy limestone	13.6	−0.4	−3.8	−27.8	27.4	3.1

(Continued on following page)

TABLE 1 | (*Continued*) C and O isotopic composition of the analyzed P-TB interval at Chaotian. The $\delta^{13}C_{org}$ values and TOC contents were reported in Saitoh et al. (2014a).

Formation	Sample ID	Lithology	Thickness (m)	$\delta^{13}C_{carb}$ vs. VPDB (‰)	$\delta^{18}O_{carb}$ vs. VPDB (‰)	$\delta^{13}C_{org}$ vs. VPDB (‰)	$\Delta^{13}C$ vs. VPDB (‰)	TOC (%)
Dalong	Dalong13	black mudstone	13.4	−1.4	−6.5	−27.0	25.6	13.4
Dalong	Dalong12	dark gray muddy limestone	13.2	−0.8	−3.8	−28.2	27.4	0.2
Dalong	Dalong11	black mudstone	13.0	−1.5	−7.2	−27.2	25.7	8.7
Dalong	Dalong10	black mudstone	12.8	−0.7	−7.1	−27.0	26.4	3.9
Dalong	Dalong9	black mudstone	12.5	0.0	−7.1	−26.4	26.4	11.9
Dalong	Dalong8	black mudstone	12.0	−0.1	−5.8	−26.4	26.2	5.6
Dalong	Dalong6	black mudstone	11.7	0.6	−6.4	−26.3	26.9	7.1
Dalong	Dalong5	black mudstone	11.2	−0.1	−5.9	−26.2	26.1	3.6
Dalong	Dalong3	black mudstone	10.8	1.2	−7.3	−26.2	27.4	4.1
Dalong	Dalong2	black mudstone	9.9	1.9	−6.3	−24.8	26.7	0.8
Dalong	Dalong1	gray mudstone	9.4	2.4	−5.7	−24.9	27.3	0.4
Wujiaping	Wujiaping20	dark gray limestone	9.0	2.9	−4.2	−26.8	29.7	0.1
Wujiaping	Wujiaping19	dark gray limestone	8.6	2.5	−6.0	−25.1	27.6	0.1
Wujiaping	Wujiaping18	dark gray limestone	8.2	3.5	−4.7	−24.9	28.4	0.1
Wujiaping	Wujiaping17	dark gray limestone	7.6	3.9	−4.1	−24.6	28.5	0.3
Wujiaping	Wujiaping16	dark gray limestone	7.2	4.2	−3.3	−22.6	26.7	0.1
Wujiaping	Wujiaping15	dark gray limestone	6.6	3.4	−4.0	−24.9	28.2	0.0
Wujiaping	Wujiaping14	dark gray limestone	6.0	3.4	−7.0	−24.5	27.8	0.1
Wujiaping	Wujiaping13	dark gray limestone	5.2	4.3	−3.0	−24.7	29.1	0.1
Wujiaping	Wujiaping12	dark gray limestone	4.6	4.1	−3.5	−24.7	28.8	0.2
Wujiaping	Wujiaping11	dark gray limestone	4.1	4.2	−3.2	−25.0	29.2	0.1
Wujiaping	Wujiaping10	dark gray limestone	3.6	3.7	−6.4	−25.0	28.7	0.1
Wujiaping	Wujiaping9	dark gray limestone	3.1	4.2	−3.4	−24.7	28.9	0.0
Wujiaping	Wujiaping8	dark gray limestone	2.6	3.9	−5.0	−23.3	27.2	0.3
Wujiaping	Wujiaping7	dark gray limestone	2.0	4.1	−4.5	−24.3	28.4	0.2
Wujiaping	Wujiaping6	dark gray limestone	1.3	3.8	−5.2	−24.3	28.2	0.4
Wujiaping	Wujiaping5	dark gray limestone	0.8	3.9	−4.4	−25.1	29.0	0.2
Wujiaping	Wujiaping4	dark gray limestone	0.0	4.1	−3.9	−24.8	28.9	0.8

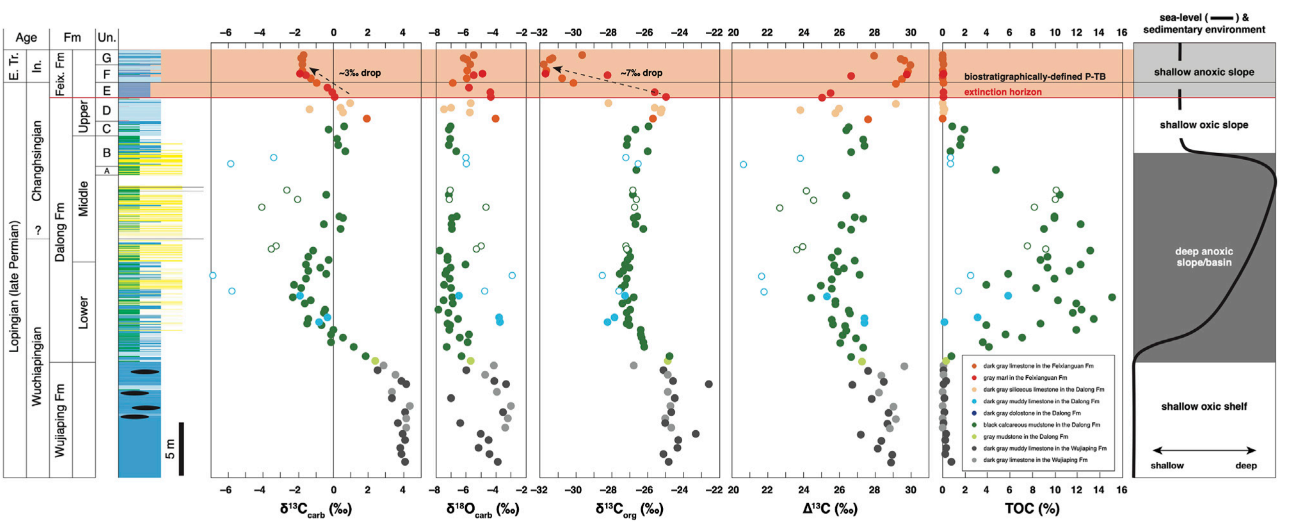

FIGURE 4 | Chemostratigraphy of the analyzed P-TB interval at Chaotian. The $\delta^{13}C_{org}$ values and TOC contents were previously reported in Saitoh et al. (2014a). Open symbols represent samples with anomalously low $\delta^{13}C_{carb}$ values in the Dalong Formation.

analyses of the P-TB carbonates in Iran, Schobben et al. (2016) suggested that the first-order $\delta^{13}C_{carb}$ trend in the bulk carbonates is robust, although small-scale isotopic fluctuations may be due to secondary alteration. In the following discussion, we focus solely on the first-order $\delta^{13}C_{carb}$ trend in the analyzed interval at Chaotian.

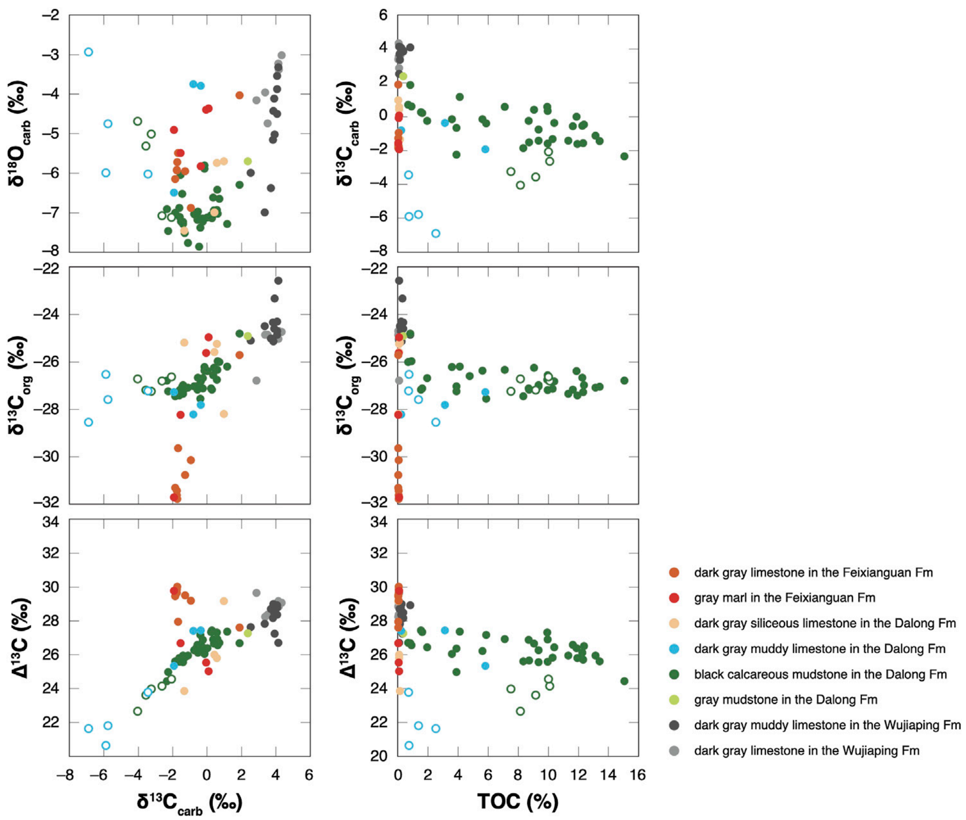

FIGURE 5 | Geochemical cross-plots of the analyzed P-TB interval at Chaotian.

DISCUSSION

$\delta^{13}C$ Stratigraphy at Chaotian

$\delta^{13}C_{carb}$ Decrease Around the Wuchiapingian-Changhsingian Boundary

The $\delta^{13}C_{carb}$ values unidirectionally decrease from ca. +4 to −2‰ across the Wujiaping/Dalong formation boundary at Chaotian (**Figure 4**). Although the timing of this negative $\delta^{13}C_{carb}$ shift is not well constrained because of the poor occurrence of index fossils, the $\delta^{13}C_{carb}$ shift likely occurred around the Wuchiapingian-Changhsingian boundary. This $\delta^{13}C_{carb}$ decrease apparently coincides with the deepening of the sedimentary setting from a shallow shelf to relatively deep slope/basin floor. However, we emphasize that carbonates in the Dalong Formation of deep-water facies comprise mainly finely fragmented bioclasts and few secondary dolomite (**Figures 3E, G–J**). Thus, regardless of the lithofacies change, this prominent $\delta^{13}C_{carb}$ decrease likely records the Lopingian secular change in the $\delta^{13}C_{DIC}$ value in the surface oceans in the eastern Paleotethys.

Two possible mechanisms could explain the $\delta^{13}C_{carb}$ decrease: 1) collapse of primary productivity in the surface oceans and 2) addition of isotopically light C into the DIC pool of the surface oceans. As certain shallow-marine taxa went extinct across the Wuchiapingian-Changhsingian boundary (e.g., Knoll et al., 1996; Bambach, 2006), extinction-related productivity deficiency may have contributed to the $\delta^{13}C_{carb}$ decrease at Chaotian. However, the magnitude of the $\delta^{13}C_{carb}$ drop (~6‰) seems to be too large to be caused solely by the collapse of primary productivity (e.g., Berner, 2002); thus the addition of ^{13}C-depleted C to the DIC pool in the surface oceans likely contributed to the $\delta^{13}C_{carb}$ drop. We emphasize that the sedimentary setting deepened from oxic shelf to anoxic slope/basin floor. The ubiquitous occurrence of small pyrite framboids in the Dalong Formation suggests the dominance of sulfate reduction in an anoxic deep-water mass on the slope/basin. The DIC in the deep-water mass would have become enriched in ^{12}C due to the anaerobic respiration; therefore, the injection of ^{13}C-depleted C into the surface oceans via shoaling of the deep-water might have contributed to the negative $\delta^{13}C_{carb}$ shift. It is noteworthy that no eruption of a large igneous province or substantial sea-level change occurred on a global scale around the Wuchiapingian-Changhsingian boundary (e.g., Haq and Schutter, 2008; Bond and Wignall, 2014). An input of volcanogenic excess CO_2 and/or reoxidized sedimentary organic C during a eustatic sea-level fall is unlikely for the cause of the $\delta^{13}C_{carb}$ drop at Chaotian.

Regional and global correlations would be useful to constrain the cause of the $\delta^{13}C_{carb}$ decrease at Chaotian. Around the

Wuchiapingian-Changhsingian boundary, a ca. 6‰ negative $\delta^{13}C_{carb}$ shift was reported at Shangsi, ca. 60 km southwest of Chaotian, in northern Sichuan (Bai et al., 2008; Shen et al. 2013), which is almost identical in magnitude to that at Chaotian. Therefore, the deep-water carbonates in northwestern South China probably record the common $\delta^{13}C_{DIC}$ decrease in eastern Paleotethys. Similar $\delta^{13}C_{carb}$ declines were also reported from other sections in South China, including Dukou in Sichuan, Shiligou in Chongqing, Zhuqiao in Hubei, and Heshan and Matan in Guangxi (Shao et al., 2000; Shen et al., 2013; Yang et al., 2019); nonetheless, the magnitude of the $\delta^{13}C_{carb}$ decreases (~2–5‰) is variable and smaller than that at Chaotian. At Abadeh in central Iran, Richoz (2006) found a negative $\delta^{13}C_{carb}$ shift in the corresponding interval in the Hambast Formation, which was later re-confirmed by Liu et al. (2013). A similar negative $\delta^{13}C_{carb}$ excursion (~4‰) was also reported from the equivalent horizons of Julfa beds/Alibashi Formation boundary at Kuh-e-Ali Bashi in northwestern Iran (Shen et al., 2013). These almost co-eval negative $\delta^{13}C_{carb}$ shifts around the Wuchiapingian-Changhsingian boundary in Iran are comparable to that at Chaotian. Moreover, a large negative $\delta^{13}C_{carb}$ excursion (~7‰) was demonstrated in the Bellerophon Formation at the Reppwand section in the Carnic Alps, Austria (Buggisch et al., 2015), which is also correlative to the negative shift at Chaotian.

A negative $\delta^{13}C_{org}$ shift, as well as the $\delta^{13}C_{carb}$ drop, around the Wuchiapingian-Changhsingian boundary has been documented in several sections in South China and Arctic Canada (e.g., Bai et al., 2008; Beauchamp et al., 2009; Wei et al., 2015; Liao et al., 2016). These $\delta^{13}C_{org}$ decreases may have likewise recorded fluctuations in the global C cycle; however, a negative $\delta^{13}C_{carb}/\delta^{13}C_{org}$ shift around the Wuchiapingian-Changhsingian boundary is not clear in the rest of the Permian world (e.g., Baud et al., 1996; Korte et al., 2004; Richoz, 2006; Baud et al., 2012). Even at the above-mentioned sections in which a negative $\delta^{13}C$ shift is recognized, the magnitude of and the trend in the $\delta^{13}C$ decrease vary substantially (Shen et al., 2013). Under the circumstances, we infer that the C cycle in the surface oceans around the Wuchiapingian-Changhsingian boundary was not globally uniform but rather widely variable possibly owing to local factors, such as primary productivity and oceanic circulation along the continental margins. More studies with high chemo- and bio-stratigraphic resolutions in various sections around the world are necessary to reveal the fluctuations in the global C cycle around the Wuchiapingian-Changhsingian boundary.

$\delta^{13}C_{carb}$ Decrease Across the P-TB

The $\delta^{13}C_{carb}$ values decrease from ca. +1 to −2‰ across the Dalong/Feixianguan formation boundary (P-TB) at Chaotian (**Figure 4**). This negative $\delta^{13}C_{carb}$ shift is identical to that previously reported at Chaotian in Cao et al. (2010). Likewise, two possible mechanisms should be considered for the cause of this $\delta^{13}C_{carb}$ decrease: 1) collapse of primary productivity in the surface oceans and 2) addition of ^{13}C-depleted C to the DIC pool in the surface oceans. The negative $\delta^{13}C_{carb}$ shift occurs across the major extinction horizon, suggesting that the shift was driven by the collapse of primary productivity during the extinction. The addition of isotopically light C to the shallow-marine DIC pool is another plausible candidate for the cause of the $\delta^{13}C_{carb}$ decrease. Isozaki et al. (2007) found frequent intercalations of thin felsic tuff layers across the extinction horizon at Chaotian and suggested volcanic stress on the shallow-marine biota during the extinction. An excess input of volcanogenic CO_2 ($\delta^{13}C$: ~−5‰) may also have contributed to the $\delta^{13}C_{carb}$ decrease. Weathering of sedimentary organic matter due to a large regression is another possible mechanism for the $\delta^{13}C_{carb}$ decrease (e.g., Yin et al., 2014). However, the sea-level drop occurred significantly before the $\delta^{13}C_{carb}$ shift at Chaotian (Isozaki et al., 2007; Saitoh et al., 2014a), without any evidence for shallowing across the extinction horizon (**Figure 4**). This suggests that a contribution of reoxidized organic C to the $\delta^{13}C_{carb}$ drop was negligible. Song et al. (2012a) proposed the existence of a large vertical $\delta^{13}C_{carb}$ gradient in the end-Permian oceans, along which a deepening of the sedimentary setting possibly caused the observed $\delta^{13}C_{carb}$ decrease. At Chaotian, however, the upper Dalong and lowermost Feixianguan carbonates across the P-TB were deposited on a relatively shallow slope without abrupt sea-level changes. Thus the $\delta^{13}C_{carb}$ decrease cannot be attributed to the assumed vertical $\delta^{13}C_{carb}$ gradient in the water column.

$\Delta^{13}C$ Increase Across the P-TB

Saitoh et al. (2014a) reported the $\delta^{13}C_{org}$ chemostratigraphy of the P-TB interval at Chaotian and revealed that the $\delta^{13}C_{org}$ values drop abruptly by 7‰ (from −25 to −32‰) immediately above the extinction horizon (**Figure 4**). This clear $\delta^{13}C_{org}$ decrease is consistent apparently with the $\delta^{13}C_{carb}$ shift documented in the present study, although the magnitude of the $\delta^{13}C_{org}$ decrease (~7‰) is substantially larger than that of the $\delta^{13}C_{carb}$ decrease (~3‰). The $\Delta^{13}C$ ($=\delta^{13}C_{carb}-\delta^{13}C_{org}$) values increase by 4‰ from +26‰ to +30‰ in the aftermath of the extinction at Chaotian. Two possible mechanisms may explain this $\Delta^{13}C$ increase: 1) an increase in C isotopic fractionation of biological C fixation and 2) additional input of ^{13}C-depleted C to the sedimentary organic matter. The high aqueous CO_2 concentration ([CO_2 (aq)]) generally promotes the large C isotopic fractionation during photosynthetic C fixation (ε_p) in the surface oceans (e.g., Rau et al., 1992, Rau et al., 1997; Kump and Arthur, 1999). The $\Delta^{13}C$ values are ~26‰ in the middle to upper Dalong Formation at Chaotian, which are consistent with the typical Calvin cycle (e.g., Schidlowski et al., 1983), although the values increase substantially to ca. 30‰ above the P-TB (**Figure 4**). It should be noted that a substantial amount of CO_2 was released during the Siberian Traps volcanism around and mostly after the P-TB (Supplementary Information) (e.g. Renne et al., 1995; Hansen, 2006; Cui et al., 2013; Cui and Kump, 2015). The increased [CO_2 (aq)] may have promoted greater ε_p (e.g., Kump and Arthur, 1999).

The previous estimates of the amount of emitted CO_2 and of the elevated pCO_2 during the Permian-Triassic transition are useful to constrain the influence of ε_p changes on the $\delta^{13}C$ records. Cui and Kump (2015) estimated that pCO_2 rose from 500 to 4,000 ppm to ~8,000 ppm during the extinction (**Supplementary Information**). Kump and Arthur (1999) derived a simplified relationship between pCO_2 and ε_p from isotopic data of modern marine algae, with some assumptions: $\varepsilon_p \approx 25–2{,}301/pCO_2$. According to this relationship, ε_p with pCO_2 of 500, 4,000, and 8,000 ppm is calculated apparently to be ~20.4, ~24.4, and ~24.7‰, respectively. Thus, the relatively large $\delta^{13}C_{org}$ decline (~7‰) compared to the $\delta^{13}C_{carb}$ decrease (~3‰) at Chaotian can be explained by the enlarged ε_p according to the elevated pCO_2. However, it is obviously difficult to extrapolate the relationship formula between pCO_2 and ε_p in Kump and Arthur (1999) directly to the end-Permian system, due to several reasons. First, several assumptions with large uncertainties are included in this simplified formula, such as the dissolved phosphate concentration in the surface seawater. Moreover, ε_p is controlled, not only by pCO_2, but also by temperature and the growth rate of phytoplankton, in general (e.g., Rau et al., 1997; Kump and Arthur, 1999). Second, this relationship formula was obtained empirically on the basis of data of modern haptophyte algae and seawater (Bidigare et al., 1997). Different coefficients on the formula would be more appropriate for the end-Permian phytoplankton communities with unknown physiology. Third, the relationship was obtained on the basis of observations of modern environments with relatively low [CO_2 (aq)] (calculated pCO_2 < 850 ppm, assuming equilibration according to Henry's Law at 25°C). It is uncertain whether the formula can be extrapolated to environments with substantially high [CO_2 (aq)], which are particularly supposed in the aftermath of the end-Permian extinction (Cui et al., 2013; Cui and Kump, 2015).

Nonetheless, the low sensitivity of ε_p to pCO_2 under high-pCO_2 conditions is probably essential (Rau et al., 1997; Kump and Arthur, 1999). Because the reciprocal dependence of ε_p on pCO_2 is attributed theoretically to isotopic discrimination by diffusion of CO_2 from the ambient seawater to the phytoplankton cell (Laws et al., 1995). It is also suggested that the sensitivity of ε_p to pCO_2 of land plants is lower than that of marine phytoplankton (e.g., Popp et al., 1989). The estimated high pCO_2 up to 4,000 ppm before the end-Permian extinction (Brand et al., 2012; Cui et al., 2013; Cui and Kump, 2015) allows us to postulate that the influence of ε_p change on the Chaotian $\delta^{13}C$ records was not significant.

Additional input of ^{13}C-depleted C to the sedimentary organic C pool is the other possible mechanism for the Chaotian P-TB $\Delta^{13}C$ increase. Rothman et al. (2014) suggested that increased Ni input to the ocean/atmosphere during the Siberian Traps volcanism promoted methanogen proliferation in the oceans ("methanogenic burst"). Methanogens generally fix C via the reductive acetyl-CoA pathway, which can produce greater C isotopic fractionation than the Calvin cycle (e.g., Preuss et al., 1989). The organic C from methanogenic biomass may have contributed, at least partly, to the $\Delta^{13}C$ increase. Terrestrial plants are another possible C source for sedimentary organic matter in the Chaotian carbonates. In general, the $\delta^{13}C_{org}$ value of Permian terrestrial plant is thought to be higher than the value of marine phytoplankton (e.g., Faure et al., 1995; Foster et al., 1997; Korte et al., 2001). Thus, if the terrestrial C flux decreased across the P-TB, the bulk $\delta^{13}C_{org}$ and $\Delta^{13}C$ values of the sediments would have decreased and increased, respectively. However, two lines of evidence exclude the possibility of the decreased terrestrial flux at Chaotian. First, as discussed above, the water depth of depositional site did not change substantially across the P-TB, and a large change in terrestrial flux owing to sea-level changes is unlikely. Second, previous studies suggested enhanced chemical weathering and increased continental flux during the Permian-Triassic transition (Algeo and Twitchett, 2010; Algeo et al., 2011; Cao et al., 2019). At Chaotian, the enhanced chemical weathering is supported by the increased supply of clay minerals/micas around the P-TB based on bulk nitrogen isotope records (Saitoh et al., 2014a). The terrestrial flux may have increased (rather than decreased) in the aftermath of the extinction, and thus the observed $\Delta^{13}C$ increase cannot be attributed to the decreased terrestrial C flux. Also, the putative vertical $\delta^{13}C_{org}$ gradient (Luo et al., 2014) cannot explain the $\Delta^{13}C$ increase because the water depth of depositional site did not change substantially across the P-TB at Chaotian.

In summary, the P-TB $\Delta^{13}C$ increase at Chaotian was most likely due to the proliferation of methanogen in the sediments during the Siberian Traps volcanism (**Figure 4**), corresponding to the "methanogenic burst" event at a local scale (Rothman et al., 2014).

Global $\delta^{13}C$ Correlations Around the P-TB

Regional $\delta^{13}C$ Differences

The $\delta^{13}C$ profile across the P-TB at Chaotian is here relatively perceived through global correlation, in the context of global C cycle during the Permian-Triassic transition. We focused particularly on the apparent magnitude of the $\delta^{13}C$ decrease across the P-TB in previous studies and examined its frequency distribution on a global scale (**Figures 6**, **7**). All the reference sections in the current compilation are summarized in **Table 2**. We categorize the compiled sections geographically into seven realms; i.e., Boreal, eastern Paleotethys, western Paleotethys, western Pangea, mid-Panthalassa, Neotethys, and Gondwana (**Figure 6**).

Marine Records

Previous $\delta^{13}C_{carb}$ studies are concentrated mostly in eastern (China) and western Tethys realms (Iran to Italy) (**Figures 6**, **7**; **Table 2**), where extensive carbonate platforms developed under warm tropical climate. These two realms share almost the same frequency distribution of the magnitude of the P-TB $\delta^{13}C_{carb}$ decrease (**Figure 7**), suggesting a common $\delta^{13}C_{DIC}$ decline throughout Paleotethys during the Permian-Triassic transition. The magnitude of the $\delta^{13}C_{carb}$ decrease ranges mostly between 3 and 6‰ in those tropical regions. In the Boreal realm, the magnitude of the P-TB $\delta^{13}C_{carb}$ decrease in few marine records is substantially large (to 19‰), which indicates a diagenetic overprint onto the original isotopic signal from seawater (Mii et al., 1997). In contrast, the magnitude of the P-TB $\delta^{13}C_{org}$ decrease varies substantially around the world (**Figures 6**, **7**). In particular, a relatively large (~7‰) $\delta^{13}C_{org}$ decline has been reported in several marine sections in high latitudes such as Greenland, Spitsbergen, Australia, and Antarctica (e.g., Retallack and Jahren, 2008; Nabbefeld et al., 2010). It is consistent with the previous notion that the magnitude of the $\delta^{13}C_{org}$ decrease in high latitudes was substantially larger than that of the $\delta^{13}C_{carb}$ decrease in equatorial regions (e.g., Krull

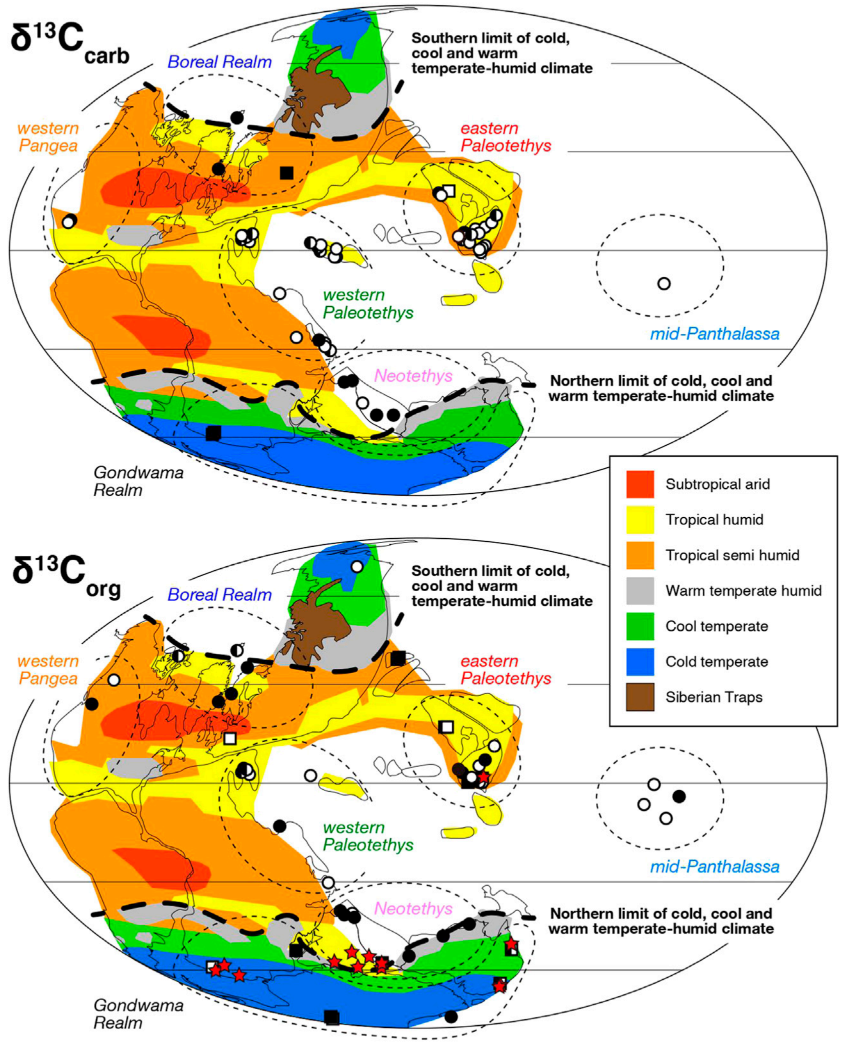

FIGURE 6 | Paleolocation map of the P-TB sections examined in inorganic (upper) and organic (lower) carbon isotope studies. Marine and terrestrial sections are shown as circles and squares, respectively. Filled and opened symbols represent sections in which the reported magnitude of the P-TB $\delta^{13}C_{carb}$ decrease is large (>5‰) and small (<5‰), respectively. A half-filled symbol represents a section in which both large and small $\delta^{13}C$ decreases were reported. A terrestrial section at which the P-TB $\delta^{13}C_{org}$ decrease is not clearly recognized is shown as a red star. The paleolocation of mid-Panthalassan sections is not precisely specified. Paleoclimate classification is after Schneebeli-Hermann (2012) and Benton and Newell (2014).

et al., 2000; Krull et al., 2004; Korte and Kozur, 2010; Payne and Clapham, 2012; Saltzman and Sedlacek, 2013; Yuan et al., 2015).

Terrestrial Records

The present $\delta^{13}C$ compilation also demonstrates that the P-TB $\delta^{13}C_{org}$ decrease is not clearly recognized in a number of terrestrial sections, especially around the Neotethys and in Gondwana realms (**Figure 6**). The $\delta^{13}C_{org}$ decline is not clearly recognized in previous studies at 14 out of 49 terrestrial sections (**Table 2**). In these sections, the $\delta^{13}C_{org}$ values are sometimes substantially scattered and no smooth $\delta^{13}C_{org}$ trend is observed (e.g., de Wit et al., 2002; Retallack et al., 2005; Coney et al., 2007). In other Gondwanan sections, the $\delta^{13}C_{org}$ decline is recognized and the apparent magnitude of the $\delta^{13}C_{org}$ decrease is mostly not large (**Figure 7**). However, the $\delta^{13}C_{org}$ decline is obscured frequently by sharp $\delta^{13}C_{org}$ drops to −45‰ (e.g., Krull and Retallack, 2000; Retallack et al., 2005).

Variable $\Delta^{13}C$ Records

Magaritz et al. (1992) originally proposed a parallel $\delta^{13}C_{carb}$ and $\delta^{13}C_{org}$ trend on the basis of the P-TB isotope profile of the Gartnerkofel Core from the Carnic Alps, Austria, and later studies confirmed similar parallel trends not only in the Tethyan but also in the Panthalassan realms (e.g., Musashi et al., 2001; Algeo et al., 2007b; Luo et al., 2014). However, other studies pointed out a decoupling between the $\delta^{13}C_{carb}$ and $\delta^{13}C_{org}$ trends around the P-TB. For example, Riccardi et al. (2007) analyzed the $\delta^{13}C_{carb}$ and $\delta^{13}C_{org}$ values of the P-TB carbonates at Meishan and Shangsi in South China, and compiled the $\Delta^{13}C$ changes during the extinction in Iran, Slovenia, Japan, Austria,

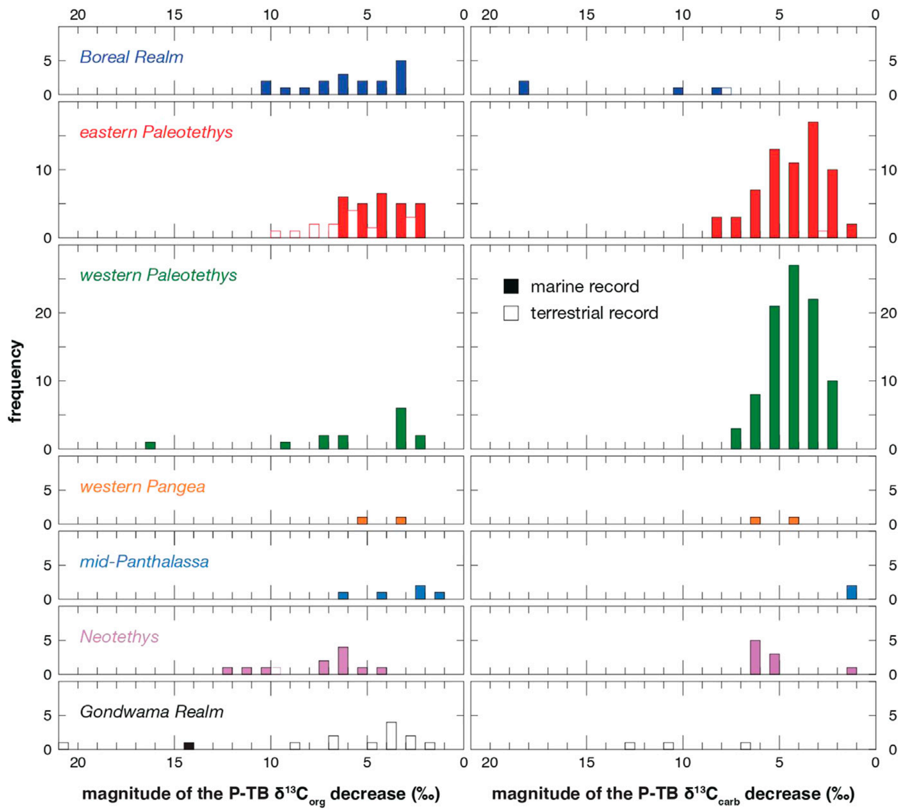

FIGURE 7 | Frequency histogram of the magnitude of the P-TB $\delta^{13}C$ decrease in various regions.

and South China. They found a $\Delta^{13}C$ decrease across the extinction horizon in these regions and suggested that it was due to proliferation of green sulfur bacteria with photic zone euxinia (e.g., Grice et al., 2005; Zhang et al., 2017). Kaiho et al. (2009) confirmed the $\Delta^{13}C$ decrease at Meishan. In contrast, the apparent $\Delta^{13}C$ increase was reported at several sections in Italy (Siegert et al., 2011), South China (Shen et al., 2012; this study), and Pakistan (Schneebeli-Hermann et al., 2013). It is difficult to reconstruct the $\Delta^{13}C$ changes in high latitudes as carbonates are generally scarce in those regions. Nonetheless, the present compilation illustrates that the $\delta^{13}C_{org}$ records are substantially variable on a global scale particularly in high latitudes, in marked contrast to the rather consistent $\delta^{13}C_{carb}$ records in equatorial Paleotethys (**Figures 6, 7**).

Potential Causes of the Marine $\delta^{13}C_{org}$ Variability

Several possible mechanisms may explain the observed $\delta^{13}C_{org}$ variability in marine records on a global scale during the Permian-Triassic transition: 1) eustatic sea-level changes, 2) intense continental weathering, 3) proliferation of green sulfur bacteria, 4) elevated pCO_2, and 5) "methanogenic burst".

Eustatic Sea-Level Changes

The $\delta^{13}C_{org}$ value of terrestrial plant was generally thought to be higher than the value of marine phytoplankton in the Permian (e.g., Faure et al., 1995; Foster et al., 1997; Korte et al., 2001). Eustatic sea-level changes during the Permian-Triassic transition may have been responsible for the $\delta^{13}C_{org}$ variability of shallow-marine records, controlling the mixing ratio of ^{13}C-enriched terrestrial and ^{13}C-depleted marine C in the shelf sediments. The Permian-Triassic transition is marked by a major transgression on a global scale (e.g., Hallam and Wignall, 1999; Erwin et al., 2002; but also see; Yin et al., 2014). It is therefore likely that shelf sediments of proximal facies shifted to be of more distal facies during the transgression, and that the terrestrial C flux to the depositional setting reduced, which resulted in the apparent $\delta^{13}C_{org}$ decrease in the bulk sediments. Although the eustatic sea-level changes could have exerted a first-order control on the global $\delta^{13}C_{org}$ variability of shallow-marine records, they do not fully explain the regionally variable $\delta^{13}C_{org}$ records. For example, the $\delta^{13}C_{org}$ records of terrestrial to marine transitional sections in western South China do not record a simple mixing of terrestrial and marine C, despite of a regional transgression, but rather the atmospheric C isotopic signal (Cui et al., 2017). Moreover, the P-TB $\delta^{13}C_{org}$ drop and $\Delta^{13}C$ increase at the present Chaotian cannot be attributed to the sea-level changes, because the water depth of depositional site did not change substantially across the P-TB, as discussed above (**Figure 4**).

Intense Continental Weathering and Increased Terrestrial C Flux

The Permian-Triassic transition is characterized by extensive vegetation collapse on lands (e.g., Retallack et al., 1996; Benton and Newell, 2014), massive soil erosion (e.g., Retallack, 2005;

Sephton et al., 2005), and intense continental weathering and increased continental flux to the oceans on a global scale (e.g., Algeo and Twitchett, 2010; Algeo et al., 2011; Cao et al., 2019). An increased flux of terrestrial plant C (with relatively high $\delta^{13}C_{org}$ value) to the shelf sediments via the vegetation collapse and intense weathering may have increased the bulk $\delta^{13}C_{org}$ values of sediments. However, this process generally decreases the bulk $\Delta^{13}C$ value of shelf carbonates and cannot explain the P-TB $\Delta^{13}C$ increase observed in several sections, including Chaotian, as discussed in the former section (**Figure 4**). Aged refractory organic matters may also have been derived into the sediments via the enhanced continental weathering and/or soil erosion (Hayes et al., 1989), though it is difficult to constrain their $\delta^{13}C_{org}$ values. On the other hand, it is most likely that a terrestrial nutrient flux to the oceans also increased simultaneously via the intense continental weathering, which stimulated eutrophication and algal blooms in the coastal oceans (e.g., Xie et al., 2007; Algeo et al., 2011; Kaiho et al., 2016). The algal blooms may have resulted in an increased flux of marine C (with relatively low $\delta^{13}C_{org}$ value) to the shelf sediments, offsetting the influence of increased terrestrial C flux on the bulk $\delta^{13}C_{org}$ value of the sediments. Because of this offset effect, the net influence of the intense continental weathering on the marine $\delta^{13}C_{org}$ records is highly uncertain.

Proliferation of Green Sulfur Bacteria With Photic Zone Euxinia

Characteristic green sulfur bacteria (GSB) may have proliferated under photic-zone euxinic conditions during the Permian-Triassic transition (e.g., Grice et al., 2005). They generally fix C via the reverse tricarboxylic acid (TCA) cycle, which can produce smaller C isotopic fractionation (~12.5‰; van Breugel et al., 2005), than the Calvin cycle (variable but mostly 25–35‰) (e.g., Schidlowski et al., 1983). Thus, the proliferation of GSB and an increased contribution of GSB biomass to the bulk organic-C pool in the shelf sediments would have decreased the $\Delta^{13}C$ value of the sediments. Riccardi et al. (2007) reported the P-TB $\Delta^{13}C$ decrease in various sections in the peri-Tethyan realm and attributed it to the GSB proliferation. Nonetheless, the proliferation of GSB cannot explain the apparent $\Delta^{13}C$ increase observed in several sections, including Chaotian (**Figure 4**).

Enlarged C Isotopic Fractionation During Photosynthesis Under the Elevated pCO₂

The increased [CO_2 (aq)] and ε_p in the surface oceans is another potential mechanism for the observed $\delta^{13}C_{carb}$-$\delta^{13}C_{org}$ decoupling (e.g., Rau et al., 1992, Rau et al., 1997). However, as discussed above for the Chaotian record, the influence of ε_p change on the P-TB $\delta^{13}C$ records may not have been significant.

Methanogenic Burst

In addition to the several potential mechanisms discussed above, we emphasize here that the "methanogenic burst" may also have contributed to the variable $\delta^{13}C_{org}$ records on a global scale (**Figures 6**, **7**). A substantial amount of Ni was presumably released into the atmosphere during the Siberian Traps volcanism (Le Vaillant et al., 2017; Rampino et al., 2017). Because Ni is a key element for microbial methanogenesis (e.g., Diekert et al., 1981), the temporary input of excess Ni was likely favorable for methanogens (e.g., Basiliko and Yavitt, 2001) and presumably enhanced microbial methanogenesis ("methanogenic burst") on a global scale (Rothman et al., 2014).

Methanogen generally fixes C via the reductive acetyl-CoA pathway, which can produce larger C isotopic fractionation up to 40‰ (e.g., Preuss et al., 1989), compared to the Calvin cycle (e.g., Schidlowski et al., 1983). Thus, according to the "methanogenic burst", the increased organic-C flux from expanded methanogen biomass to the bulk organic-C pool in the local sediments may have caused the large $\delta^{13}C_{org}$ decrease (**Figures 6**, **7**). However, the activity of methanogen is generally regulated, not only by the Ni availability, but also by a number of environmental factors, such as temperature, CO_2 levels, and availability of organic substrates (**Supplementary Information**; e.g., Singh et al., 2010; Nazaries et al., 2013). Although the excess Ni input during the Siberian Traps volcanism likely promoted methanogenesis, the variable activity of methanogen in the local sediments may have been responsible for the observed $\delta^{13}C_{org}$ variability on a global scale. The elevated temperature and pCO_2 may also have stimulated the "methanogenic burst", because these factors generally increase the biogenic CH_4 emissions in various environments (**Supplementary Information**; e.g., van Groenigen et al., 2011; Yvon-Durocher et al., 2014; Aben et al., 2017). The "methanogenic burst" may have occurred not only in marine sediments but also in terrestrial wetlands (**Figure 8**). Nonetheless, it is still difficult to estimate the total amount of released Ni during the Siberian Traps volcanism (Le Vaillant et al., 2017), and to evaluate the influence of the "methanogenic burst" on the global $\delta^{13}C_{org}$ records quantitatively.

In summary, the P-TB $\delta^{13}C_{org}$ variability in marine records on a global scale may have been attributed to several potential mechanisms, including the eustatic sea-level changes, intense continental weathering, and GSB proliferation. We infer that the "methanogenic burst" was also involved, at least in part, in the substantial $\delta^{13}C_{org}$ decrease in several sections, including the present Chaotian (**Figure 4**).

Implications for the Global CH_4 Cycle in the Aftermath of the Extinction

A substantial amount of CH_4 was presumably released into the atmosphere during the Siberian Traps volcanism (**Figure 8B**), via volcanic intrusion into coal (e.g., Retallack and Krull, 2006; Retallack and Jahren, 2008; Grasby et al., 2011; Shen et al., 2012; Rampino et al., 2017; Elkins-Tanton et al., 2020), and via destabilization of submarine and permafrost clathrates (e.g., Krull et al., 2000; Krull et al., 2004). Pyrogenic CH_4 was also produced by the incomplete combustion of organic carbon (e.g., Kirschke et al., 2013) and emitted during extensive wildfire events around the P-TB both in the northern and southern hemispheres (e.g., Shen et al., 2011b; Hudspith et al., 2014; Vajda et al., 2020). The "methanogenic burst" likely contributed to the elevated pCH_4 (Rothman et al., 2014). The claimed Araguainha impact event in Brazil (Tohver et al., 2013)

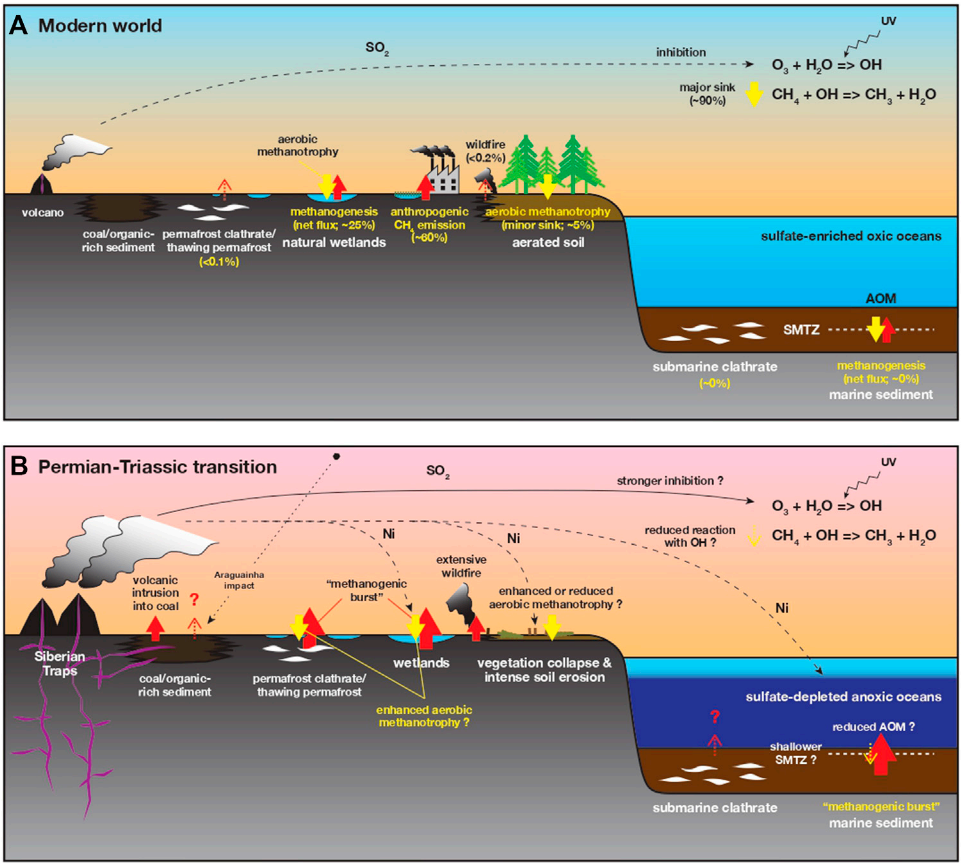

FIGURE 8 | Schematic diagram of the global CH_4 cycle in the modern world **(A)** and during the Permian-Triassic transition **(B)**. CH_4 influx to and efflux from the atmosphere are shown as red and yellow arrows, respectively. In the modern system, the global atmospheric CH_4 budget is 0.4–0.5 Gt C/year (Supplementary Information; e.g., Conrad, 2009; Nazaries et al., 2013). During the Permian-Triassic transition, several processes may have contributed to the elevated pCH_4 and climate warming, although terrestrial responses to the elevated pCH_4 were probably complex. The elevated pCH_4 enhanced aerobic methanotrophy in local soils whereas the intense soil erosion decreased a net CH_4 efflux in the global budget. AOM: anaerobic oxidation of methane; SMTZ: sulfate-methane transition zone. See **Supplementary Information** for details.

may also have contributed to the CH_4 accumulation in the atmosphere, though its timing, magnitude, and effective time span for the global CH_4 cycle are not well-constrained. Together with other greenhouse gases like CO_2, the elevated pCH_4 may have contributed to the climate warming during the earliest Triassic (e.g., Hallam and Wignall, 1997; Joachimski et al., 2012; Sun et al., 2012; Cui and Kump, 2015), although the long-term warming may have been disturbed intermittently by short-term SO_2-induced cooling (Black et al., 2018).

Although there still remains large uncertainty, we infer fluctuations in the global CH_4 cycle in the aftermath of the extinction based on the present and previous observations (**Figure 8B**). Firstly, aerobic methanotrophy may have prevailed in aerated terrestrial soils in the Gondwana and peri-Gondwanan realms (**Figure 8B**; Krull and Retallack, 2000). The present compilation illustrates that the P-TB $\delta^{13}C_{org}$ decrease is not clearly recognized in a number of terrestrial sections, especially around the Neotethys and in Gondwana realms (**Figure 6**; **Table 2**). The highly scattered and variable $\delta^{13}C_{org}$ records in the terrestrial successions were likely due to local-scale and short-term organic C dynamics in soils, including vegetation, selective microbial decomposition of sedimentary organic matters with C isotopic fractionation, and addition of microbial biomass to the sedimentary C pool (e.g., Krull and Retallack, 2000; Korte and Kozur, 2010). The locally enhanced methanotrophy might have been involved, at least in part, in the soil C dynamics and in the scattered $\delta^{13}C_{org}$ records in the Gondwana and peri-Gondwanan realms (Krull and Retallack, 2000), possibly according to the warming and permafrost thaw (**Supplementary Information**; e.g., Oh et al., 2020).

Secondly, the oceanic sediments may have been a significantly large source for atmospheric CH_4 at that time. In the modern oceans enriched in sulfate (the SO_4^{2-} concentration = 28 mM), almost all CH_4, produced in deeper sediments, is consumed by anaerobic oxidation of methane (AOM) in the sulfate-methane transition zone (SMTZ) (**Figure 8**; **Supplementary Information**; e.g., Reeburgh, 2007). However, AOM would be substantially suppressed when the sulfate concentration is <0.5 mM (Knittel and Boetius, 2009). The Permian-Triassic transition interval is characterized by the substantially low sulfate concentration in the oceans (0.6–2.8 mM) (Luo et al., 2010; Schobben et al., 2017; Stebbins et al., 2019). This estimated SO_4^{2-} range is slightly higher than the threshold of the AOM rate. Nonetheless, the porewater sulfate concentration in the sediments may have quickly become <0.5 mM at a very shallow depth, due to sulfate consumption via decomposition of other organic substrates. The sedimentary AOM was consequently suppressed and the oceanic sediments might have been a larger CH_4 source compared to in the modern oceans, further contributing to the elevated pCH_4. The impact of "methanogenic burst" on the enhanced CH_4 emissions should have been significant under such sulfate-depleted conditions with less AOM. Prevailing oceanic anoxia (e.g., Wignall and Hallam, 1992; Isozaki, 1997; Song et al., 2012b) also helped CH_4 to escape from the oceans to the atmosphere (e.g., Ryskin, 2003).

Finally, the global CH_4 budgets may have been disturbed by the terrestrial devastation and intense continental weathering (e.g., Algeo and Twitchett, 2010; Cao et al., 2019). The Permian-Triassic transition is characterized by the extensive vegetation collapse on lands and massive soil erosion on a global scale (**Figure 8B**; e.g., Retallack, 2005; Sephton et al., 2005; Benton and Newell, 2014). The destruction of terrestrial ecosystems and the decay of land plants in the aftermath of the extinction was claimed to bring the well-known Early Triassic "coal gap" (Retallack et al., 1996). Although the release of substantial amounts of Ni into the ocean-atmosphere during the Siberian Traps volcanism may have caused the "methanogenic burst", it may also have contributed to the vegetation collapse because excess Ni is generally toxic to plants (Fielding et al., 2019). The vegetation collapse could have stimulated the destabilization of permafrost and the CH_4 emissions in high latitudes according to the warming (Nauta et al., 2015), whereas the massive soil erosion might also have contributed to the atmospheric CH_4 accumulation as aerated terrestrial soils are a CH_4 sink (**Supplementary Information**; **Figure 8B**).

CONCLUSIONS

The carbon isotopic composition of carbonate ($\delta^{13}C_{carb}$) across the Permian-Triassic boundary (P-TB) was analyzed at Chaotian, Sichuan, South China, and was correlated to the chemostratigraphy of the carbon isotopic composition of organic carbon ($\delta^{13}C_{org}$) of the same interval. The $\delta^{13}C_{carb}$ and $\delta^{13}C_{org}$ records at Chaotian were further integrated into the records from various marine and terrestrial environments all around the world, to examine fluctuations in the global methane (CH_4) cycle during the Permian-Triassic transition. The following results were obtained:

(1) The $\delta^{13}C_{carb}$ values decrease from ca. +1 to −2‰ across the P-TB, possibly reflecting the shallow-marine extinction and the collapse of primary productivity in the oceans. The frequent intercalation of felsic tuff layers around the extinction horizon suggests that volcanic activity also contributed to the $\delta^{13}C_{carb}$ decrease.
(2) The magnitude of the $\delta^{13}C_{carb}$ decline (~3‰) is substantially smaller than the magnitude of the $\delta^{13}C_{org}$ decrease (~7‰) across the P-TB. This $\delta^{13}C_{carb}$-$\delta^{13}C_{org}$ decoupling could be explained by an elevated CO_2 concentration in the ocean/atmosphere and/or proliferation of methanogen ("methanogenic burst") in the sediments, according to the Siberian Traps volcanism.
(3) A global P-TB $\delta^{13}C$ compilation shows a large variation in marine $\delta^{13}C_{org}$ records, which could be attributed to several potential mechanisms including eustatic sea-level changes and proliferation of green sulfur bacteria. We infer that the "methanogenic burst" may also have contributed, at least in part, to the $\delta^{13}C_{org}$ variability. The global CH_4 cycle might have fluctuated substantially in the aftermath of the extinction.

DATA AVAILABILITY STATEMENT

The original contributions presented in the study are included in the article/**Supplementary Material**, further inquiries can be directed to the corresponding author.

AUTHOR CONTRIBUTIONS

MS designed the study. YI provided the samples for the analyses. MS and YI conducted the lithofacies description. MS conducted the isotopic analyses. MS and YI wrote the manuscript.

FUNDING

This study was supported by JSPS KAKENHI (16204040, 20224012, 26610159, and 15H03740).

ACKNOWLEDGMENTS

Naomi Takahashi assisted with the isotopic analyses. Shuzhong Shen and two anonymous reviewers provided constructive comments that improved the article.

SUPPLEMENTARY MATERIAL

The Supplementary Material for this article can be found online at: https://www.frontiersin.org/articles/10.3389/feart.2020.596178/full#supplementary-material.

REFERENCES

Aben, R. C. H., Barros, N., van Donk, E., Frenken, T., Hilt, S., Kazanjian, G., et al. (2017). Cross continental increase in methane ebullition under climate change. *Nat. Commun*. 8, 1682. doi:10.1038/s41467-017-01535-y

Algeo, T. J., Chen, Z. Q., Fraiser, M. L., and Twitchett, R. J. (2011). Terrestrial–marine teleconnections in the collapse and rebuilding of Early Triassic marine ecosystems. *Palaeogeogr. Palaeoclimatol. Palaeoecol*. 308, 1–11. doi:10.1016/j.palaeo.2011.01.011

Algeo, T. J., Ellwood, B., Nguyen, T. K. T., Rowe, H., and Maynard, J. B. (2007a). The Permian– Triassic boundary at Nhi Tao, Vietnam: evidence for recurrent influx of sulfidic watermasses to a shallow-marine carbonate platform. *Palaeogeogr. Palaeoclimatol. Palaeoecol*. 252, 304–327. doi:10.1016/j.palaeo.2006.11.055

Algeo, T. J., Hannigan, R., Rowe, H., Brookfield, M., Baud, A., Krystyn, L., et al. (2007b). Sequencing events across the permian–triassic boundary, guryul ravine (Kashmir, India). *Palaeogeogr. Palaeoclimatol. Palaeoecol*. 252, 328–346. doi:10.1016/j.palaeo.2006.11.050

Algeo, T. J., Henderson, C. M., Ellwood, B., Rowe, H., Elswick, E., Bates, S., et al. (2012). Evidence for a diachronous Late Permian marine crisis from the Canadian Arctic region. *GSA Bull*. 124, 1424–1448. doi:10.1130/B30505.1

Algeo, T. J., Shen, Y., Zhang, T. G., Lyons, T. W., Bates, S., Rowe, H., et al. (2008). Association of ^{34}S-depleted pyrite layers with negative carbonate δ^{13}C excursions at the Permian-Triassic boundary: evidence for upwelling of sulfidic deep-ocean water masses. *Geochem. Geophys. Geosyst*. 9, Q04025. doi:10.1029/2007GC001823

Algeo, T. J., and Twitchett, R. J. (2010). Anomalous Early Triassic sediment fluxes due to elevated weathering rates and their biological consequences. *Geology*. 38, 1023–1026. doi:10.1130/G31203.1

Alroy, J. (2010). The shifting balance of diversity among major marine animal groups. *Science* 276, 235–238. doi:10.1126/science.1189910

Bagherpour, B., Bucher, H., Vennemann, T., Schneebeli-Hermann, E., Yuan, D. X., Leu, M., et al. (2019). Are Late Permian carbon isotope excursions of local or of global significance? *GSA Bull*. 132, 521–544. doi:10.1130/B31996.1

Bai, X., Luo, G. M., Wu, X., Wang, Y. Z., Huang, J. H., and Wang, X. J. (2008). Carbon isotope records indicative of paleoceanographical events at the latest permian Dalong formation at Shangsi, northeast sichuan, China. *J. Chin. Univ. Geosci*. 19, 481–487. doi:10.1016/S1002-0705(08)60053-9

Bambach, R. K. (2006). Phanerozoic biodiversity mass extinctions. *Ann. Rev. Earth Planet. Sci*. 34, 127–155. doi:10.1146/annurev.earth.33.092203.122654

Baresel, B., Bucher, H., Bagherpour, B., Brosse, M., Guodun, K., and Schaltegger, U. (2017). Timing of global regression and microbial bloom linked with the Permian-Triassic boundary mass extinction: implications for driving mechanisms. *Sci. Rep*. 7:43630. doi:10.1038/srep43630

Basiliko, N., and Yavitt, J. B. (2001). Influence of Ni, Co, Fe, and Na additions on methane production in Sphagnum-dominated Northern American peatlands. *Biogeochemistry* 52, 133–153. doi:10.1023/A:1006461803585

Baud, A., Atudorei, V., and Sharp, Z. (1996). Late Permian and Early Triassic evolution of the Northern Indian margin: carbon isotope and sequence stratigraphy. *Geodinam. Acta* 9, 57–77. doi:10.1080/09853111.1996.11105278

Baud, A., Magaritz, M., and Holser, W. T. (1989). Permian–Triassic of the Tethys: carbon isotope studies. *Geol. Rundsch*. 78, 649–677.

Baud, A., Richoz, S., Beauchamp, B., Cordey, F., Grasby, S., Henderson, C. M., et al. (2012). The buday'ah formation, sultanate of Oman: a middle permian to early triassic oceanic record of the Neotethys and the late induan microsphere bloom. *J. Asian Earth Sci*. 43, 130–144. doi:10.1016/j.jseaes.2011.08.016

Beauchamp, B., Henderson, C. M., Grasby, S. E., Gates, L. T., Beatty, T. W., Utting, J., et al. (2009). Late permian sedimentation in the Sverdrup Basin, Canadian Arctic: the lindström and black stripe formations. *Bull. Can. Petrol. Geol*. 57, 167–191. doi:10.2113/gscpgbull.57.2.167

Becker, L., Poreda, R. J., Basu, A. R., Pope, K. O., Harrison, T. M., Nicholson, C., et al. (2004). Bedout: a possible end-Permian impact crater offshore of northwestern Australia. *Science* 304, 1469–1476. doi:10.1126/science.1093925

Benton, M. J., and Newell, A. J. (2014). Impacts of global warming on Permo-Triassic terrestrial ecosystems. *Gondwana Res*. 25, 1308–1337. doi:10.1016/j.gr.2012.12.010

Berner, R. A. (2002). Examination of hypotheses for the Permo–Triassic boundary extinction by carbon cycle modeling. *Proc. Natl. Acad. Sci. USA* 99, 4172–4177. doi:10.1073/pnas.032095199

Bidigare, R. R., Fluegge, A., Freeman, K. H., Hanson, K. L., Hayes, J. M., Hollander, D., et al. (1997). Consistent fractionation of ^{13}C in nature and in the laboratory: growth-rate effects in some haptophyte algae. *Glob. Biogeochem. Cycles* 11, 279–292. doi:10.1029/96gb03939

Black, B. A., Neely, R. R., Lamarque, J., Elkins-Tanton, L. T., Kiehl, J. T., Shields, C. A., et al. (2018). Systemic swings in end-Permian climate from Siberian Traps carbon and sulfur outgassing. *Nat. Geosci*. 11, 949–954. doi:10.1038/s41561-018-0261-y

Bond, D. P. G., and Wignall, P. B. (2014). "Large igneous provinces and mass extinctions: an update." in *Volcanism, impacts, and mass extinctions: causes and effects. Spec. Pap*., Editors G. Keller and A. C. Kerr, Geol. Soc. Am. Vol 505, 29–55. doi:10.1130/2014.2505(02)

Brand, U., Blamey, N., Garbelli, C., Griesshaber, E., Posenato, R., Angiolini, L., et al. (2016). Methane Hydrate: killer cause of Earth's greatest mass extinction. *Palaeoworld* 25, 496–507. doi:10.1016/j.palwor.2016.06.002

Brand, U., Posenato, R., Came, R., Affek, H., Angiolini, L., Azmy, K., et al. (2012). The end-Permian mass extinction: a rapid volcanic CO_2 and CH_4-climatic catastrophe. *Chem. Geol*. 322-323, 121–144. doi:10.1016/j.chemgeo.2012.06.015

Buggisch, W., Krainer, K., Schaffhauser, M., Joachimski, M., and Korte, C. (2015). Late Carboniferous to Late Permian carbon isotope stratigraphy: A new record from post-Variscan carbonates from the Southern Alps (Austria and Italy). *Palaeogeogr. Palaeoclimatol. Palaeoecol*. 433, 174–190. doi:10.1016/j.palaeo.2015.05.012

Burgess, S. D., and Bowring, S. A. (2015). High-precision geochronology confirms voluminous magmatism before, during, and after Earth's most severe extinction. *Sci. Adv*. 1:e1500470. doi:10.1126/sciadv.1500470

Campbell, I. H., Czamanske, G. K., Fedorenko, V. A., Hill, R. I., and Stepanov, V. (1992). Synchronism of the siberian traps and the permian-triassic boundary. *Science* 258, 1760–1763. doi:10.1126/science.258.5089.1760

Cao, C. Q., Wang, W., and Jin, Y. G. (2002). Carbon isotope excursions across the permian-triassic boundary in the meishan section, zhejiang province, China. *Chin. Sci. Bull*. 47, 1125–1129.

Cao, C. Q., Yang, Y. C., Shen, S. Z., Wang, W., Zheng, Q. F., and Summons, R. E. (2010). Pattern of $\delta^{13}C_{carb}$ and implications for geological events during the Permian-Triassic transition in South China. *Geol. J*. 45, 186–194. doi:10.1002/gj.1220

Cao, Y., Song, H., Algeo, T. J., Chu, D., Du, Y., Tian, L., et al. (2019). Intensified chemical weathering during the Permian-Triassic transition recorded in terrestrial and marine successions. *Palaeogeogr. Palaeoclimatol. Palaeoecol*. 519, 166–177. doi:10.1016/j.palaeo.2018.06.012

Clapham, M. E., and Payne, J. L. (2011). Acidification, anoxia, and extinction: a multiple logistic regression analysis of extinction selectivity during the Middle and Late Permian. *Geology* 39, 1059–1062. doi:10.1130/G32230.1

Clarkson, M. O., Kasemann, S. A., Wood, R. A., Lenton, T. M., Daines, S. J., Richoz, S., et al. (2015). Ocean acidification and the Permo-Triassic mass extinction. *Science* 348, 229–232. doi:10.1126/science.aaa0193

Coney, L., Reimold, W. U., Hancox, P. J., Mader, D., Koeberl, C., McDonald, I., Struck, U., Vajda, V., and Kamo, S. L. (2007). Geochemical and mineralogical investigation of the Permian–Triassic boundary in the continental realm of the southern Karoo Basin, South Africa. *Palaeoworld Rep*. 16, 67–104.

Conrad, R. (2009). The global methane cycle: recent advances in understanding the microbial processes involved. *Environ. Microbiol. Rep*. 1, 285–292.doi:10.1111/j.1758-2229.2009.00038.x

Cui, Y., Bercovici, A., Yu, J. X., Kump, L. R., Freeman, K. H., Su, S. G., et al. (2017). Carbon cycle perturbation expressed in terrestrial Permian–Triassic boundary sections in South China. *Glob. Planet. Change* 148, 272–285. doi:10.1016/j.gloplacha.2015.10.018

Cui, Y., and Kump, L. R. (2015). Global warming and the end-Permian extinction event: proxy and modeling perspectives. *Earth-Sci. Rev*. 149, 5–22. doi:10.1016/j.earscirev.2014.04.007

Cui, Y., Kump, L. R., and Ridgwell, A. (2013). Initial assessment of the carbon emission rate and climatic consequences during the end-Permian mass extinction. *Palaeogeogr. Palaeoclimatol. Palaeoecol*. 389, 128–136. doi:10.1016/j.palaeo.2013.09.001

de Wit, M. J., Ghosh, J. G., de Villiers, S., Rakotosolofo, N., Alexander, J., Tripathi, A., et al. (2002). Multiple organic carbon isotope reversals across the Permian–

Triassic boundary of terrestrial Gondwana Sequences: clues to extinction patterns and delayed ecosystem recovery. *J. Geol.* 110, 227–240.

Diekert, G., Konheiser, U., Piechulla, K., and Thauer, R. K. (1981). Nickel requirement and factor F430 content of methanogenic bacteria. *J. Bacteriol.* 148, 459–464.

Elkins-Tanton, L. T., Grasby, S. E., Black, B. A., Veselovskiy, R. V., Ardakani, O. H., and Goodarzi, F. (2020). Field evidence for coal combustion links the 252 Ma Siberian Traps with global carbon disruption. *Geology* 48, 986–991. doi:10.1130/G47365.1

Erwin, D. H., Bowring, S. A., and Yugan, J. (2002). "End-Permian mass extinctions: a review." in *Catastrophic events and mass extinctions: impacts and beyond: boulder, Colorado*. Editors C. Koeberl, and K. G. MacLeod, (Boulder: Geol. Soc. Am. Spec. Pap.) 356, pp. 363–383.

Erwin, D. H. (2006). *Extinction; how life on Earth nearly ended 250 million years ago*. New Jersey, United States: Princeton Univ. Press, 296 p.

Erwin, D. H. (1993). *The great paleozoic crisis*. New York, United States: Columbia Univ. Press, 327 p.

Faure, K., de Wit, M. J., and Willis, J. P. (1995). Late Permian global coal hiatus linked to ^{13}C-depleted CO_2 flux into the atmosphere during the final consolidation of Pangea. *Geology* 23, 507–510.

Fielding, C. R., Frank, T. D., McLoughlin, S., Vajda, V., Mays, C., Tevyaw, A. P., et al. (2019). Age and pattern of the southern high-latitude continental end-Permian extinction constrained by multiproxy analysis. *Nat. Commun.* 10:385. doi:10.1038/s41467-018-07934-z

Foster, C. B., Logan, G. A., Summons, R. E., Gorter, J. D., and Edwards, D. S. (1997). Carbon isotopes, kerogen types and the Permian–Triassic boundary in Australia: implications for exploration. *Aus. Petrol. Product. Explor. Assoc. J.* 37, 472–489.

Garbelli, C., Angiolini, L., and Shen, S. Z. (2017). Biomineralization and global change: a new perspective for understanding the end-Permian extinction. *Geology* 45, 19–22. doi:10.1130/G38430.1

Gastaldo, R. A., Kamo, S. L., Neveling, J., Geissman, J. W., Looy, C. V., and Martini, A. M. (2020). The base of the lystrosaurus assemblage zone, karoo basin, predates the end-permian marine extinction. *Nat. Commun.* 11, 1428. doi:10.1038/s41467-020-15243-7

Grasby, S. E., and Beauchamp, B. (2008). Intrabasin variability of the carbon-isotope record across the permian–triassic transition, sverdrup basin, arctic Canada. *Chem. Geol.* 253, 141–150. doi:10.1016/j.chemgeo.2008.05.005

Grasby, S. E., Sanei, H., and Beauchamp, B. (2011). Catastrophic dispersion of coal fly ash into oceans during the latest Permian extinction. *Nat. Geosci.* 4, 104–107. doi:10.1038/ngeo1069

Grice, K., Cao, C. Q., Love, G. D., Böttcher, M. E., Twitchett, R. J., Grosjean, E., et al. (2005). Photic zone euxinia during the Permian-Triassic superanoxic event. *Science*. 307, 706–709. doi:10.1126/science.1104323

Hallam, A., and Wignall, P. B. (1999). Mass Extinctions and sea-level changes. *Earth-Sci. Rev.* 48, 217–250. doi:10.1016/S0012-8252(99)00055-0

Hallam, A., and Wignall, P. B. (1997). *Mass extinctions and their aftermath*. Oxford, UK: Oxford Univ. Press, 320 p.

Hansen, H. J. (2006). Stable isotopes of carbon from basaltic rocks and their possible relation to atmospheric isotope excursions. *Lithos* 92, 105–116. doi:10.1016/j.lithos.2006.03.029

Haq, B. U., and Schutter, S. R. (2008). A chronology of paleozoic sea-level changes. *Science* 322, 64–68. doi:10.1126/science.1161648

Hayes, J. M., Popp, B. N., Takigiku, R., and Johnson, M. W. (1989). An isotopic study of biogeochemical relationships between carbonates and organic carbon in the Greenhorn Formation. *Geochim. Cosmochim. Acta* 53, 2961–2972.

Hayes, J. M., Strauss, H., and Kaufman, A. J. (1999). The abundance of ^{13}C in marine organic matter and isotopic fractionation in the global biogeochemical cycle of carbon during the past 800 Ma. *Chem. Geol.* 161, 103–125. doi:10.1016/S0009-2541(99)00083-2

Heydari, E., and Hassanzadeh, J. (2003). Deev Jahi Model of the Permian–Triassic boundary mass extinction: a case for gas hydrates as the main cause of biological crisis on Earth. *Sed. Geol.* 163, 147–163. doi:10.1016/j.sedgeo.2003.08.002

Heydari, E., Wade, W. J., and Hassanzadeh, J. (2001). Diagenetic origin of carbon and oxygen isotope compositions of Permian–Triassic boundary strata. *Sed. Geol.* 143, 191–197. doi:10.1016/S0037-0738(01)00095-1

Holser, W. T., Schönlaub, H.-P., Attrep, M., Boeckelmann, K., Klein, P., Magaritz, M., et al. (1989). A unique geochemical record at the Permian/Triassic boundary. *Nature* 337, 39–44.

Horacek, M., Brandner, R., and Abart, R. (2007b). Carbon isotope record of the P/T boundary and the Lower Triassic in the Southern Alps: evidence for rapid changes in storage of organic carbon. *Palaeogeogr. Palaeoclimatol. Palaeoecol.* 252, 347–354. doi:10.1016/j.palaeo.2006.11.049

Horacek, M., Richoz, S., Brandner, R., Krystyn, L., and Spötl, C. (2007a). Evidence for recurrent changes in Lower Triassic oceanic circulation of the Tethys: the $\delta^{13}C$ record from marine sections in Iran. *Palaeogeogr. Palaeoclimatol. Palaeoecol.* 252, 355–369. doi:10.1016/j.palaeo.2006.11.052

Hudspith, V. A., Rimmer, S. M., and Belcher, C. M. (2014). Latest Permian chars may derive from wildfires, not coal combustion. *Geology* 42, 879–882. doi:10.1130/G35920.1

Isozaki, Y. (2019). "End-paleozoic mass extinction: hierarchy of causes and a new cosmoclimatological perspective for the largest crisis." in *Astrobiology*. Editors A. Yamagishi, T. Kakegawa, and T. Usui. (Singapore: Springer), 273–301. doi:10.1007/978-981-13-3639-3_18

Isozaki, Y. (1997). Permo-Triassic boundary Superanoxia and stratified superocean: records from lost deep-sea. *Science* 276, 235–238. doi:10.1126/science.276.5310.235

Isozaki, Y., Shimizu, N., Yao, J. X., Ji, Z. S., and Matsuda, T. (2007). End-Permian extinction and volcanism-induced environmental stress: the Permian-Triassic boundary interval of lower-slope facies at Chaotian, South China. *Palaeogeogr. Palaeoclimatol. Palaeoecol.* 252, 218–238. doi:10.1016/j.palaeo.2006.11.051

Isozaki, Y., Yao, J. X., Ji, Z. S., Saitoh, M., Kobayashi, N., and Sakai, H. (2008). Rapid sea-level change in the late guadalupian (permian) on the tethyan side of South China: litho- and biostratigraphy of the chaotian section in sichuan. *Proc. Jpn. Acad. Ser. B.* 84, 344–353. doi:10.2183/pjab/84.344

Isozaki, Y., Yao, J. X., Matsuda, T., Sakai, H., Ji, Z. S., Shimizu, N., et al. (2004). Stratigraphy of the middle-upper permian and lowermost triassic at chaotian, sichuan, China. –Record of late permian double mass extinction event–. *Proc. Jpn. Acad. Ser. B.* 80, 10–16. doi:10.2183/pjab.80.10

Ji, Z. S., Yao, J. X., Isozaki, Y., Matsuda, T., and Wu, G. C. (2007). Conodont biostratigraphy across the permian-triassic boundary at chaotian, in northern sichuan, China. *Palaeogeogr. Palaeoclimatol. Palaeoecol.* 252, 39–55. doi:10.1016/j.palaeo.2006.11.033

Jin, Y. G., Mei, S. L., Wang, W., Wang, X. D., Shen, S. Z., Shang, Q. H., et al. (1998). On the Lopingian series of the Permian system. *Palaeoworld* 9, 1–18.

Jin, Y. G., Wang, Y., Wang, W., Shang, Q. H., Cao, C. Q., and Erwin, D. H. (2000). Pattern of marine mass extinction near the Permian–Triassic boundary in South China. *Science* 289, 432–436. doi:10.1126/science.289.5478.432

Joachimski, M. M., Alekseev, A. S., Grigoryan, A., and Gatovsky, Y. A. (2020). Siberian Trap volcanism, global warming and the Permian-Triassic mass extinction: new insights from Armenian Permian-Triassic sections. *GSA Bull.* 132, 427–443. doi:10.1130/B35108.1

Joachimski, M. M., Lai, X. L., Shen, S. Z., Jiang, H. S., Luo, G. M., Chen, B., et al. (2012). Climate warming in the latest Permian and the Permian-Triassic mass extinction. *Geology* 40, 195–198. doi:10.1130/G32707.1

Jost, A. B., Mundil, R., He, B., Brown, S. T., Altiner, D., Sun, Y. D., et al. (2014). Constraining the cause of the end-Guadalupian extinction with coupled records of carbon and calcium isotopes. *Earth Planet Sci. Lett.* 396, 201–212. doi:10.1016/j.epsl.2014.04.014

Jurikova, H., Gutjahr, M., Wallmann, K., Flögel, S., Liebetrau, V., Posenato, R., et al. (2020). Permian–Triassic mass extinction pulses driven by major marine carbon cycle perturbations. *Nat. Geosci.* 13, 745–750. doi:10.1038/s41561-020-00646-4

Kaiho, K., Chen, Z. Q., and Sawada, K. (2009). Possible causes for a negative shift in the stable carbon isotope ratio before, during and after the end-Permian mass extinction in Meishan, South China. *Aus. J. Earth Sci.* 56, 799–808. doi:10.1080/08120090903002615

Kaiho, K., Saito, R., Ito, K., Miyaji, T., Biswas, R., Tian, L., et al. (2016). Effects of soil erosion and anoxic–euxinic ocean in the Permian–Triassic marine crisis. *Heliyon* 2, e00137. doi:10.1016/j.heliyon.2016.e00137

Kajiwara, Y., Yamakita, S., Ishida, K., Ishiga, H., and Imai, A. (1994). Development of a largely anoxic stratified ocean and its temporary massive mixing at the Permian/Triassic boundary supported by the sulfur isotopic record.

Palaeogeogr. Palaeoclimatol. Palaeoecol. 111, 367–379. doi:10.1016/0031-0182(94)90072-8

Kamo, S. L., Czamanske, G. K., Amelin, Y., Fedorenko, V. A., Davis, D. W., and Trofimov, V. R. (2003). Rapid eruption of Siberian flood-volcanic rocks and evidence for coincidence with the Permian–Triassic boundary and mass extinction at 251 Ma. *Earth Planet Sci. Lett.* 214 (1–2), 75–91. doi:10.1016/S0012-821X(03)00347-9

Kidder, D. L., and Worsley, T. R. (2004). Causes and consequences of extreme Permo-Triassic warming to globally equable climate and relation to the Permo-Triassic extinction and recovery. *Palaeogeogr. Palaeoclimatol. Palaeoecol.* 203, 207–237. doi:10.1016/S0031-0182(03)00667-9

Kirschke, S., Bousquet, P., Ciais, P., Saunois, M., Canadell, J. G., Dlugokencky, E. J., et al. (2013). Three decades of global methane sources and sinks. *Nat. Geosci.* 6, 813–823. doi:10.1038/ngeo1955

Knauth, L. P., and Kennedy, M. J. (2009). The late Precambrian greening of the Earth. *Nature* 460, 728–732. doi:10.1038/nature08213

Knittel, K., and Boetius, A. (2009). Anaerobic oxidation of methane: progress with an unknown process. *Ann. Rev. Microbiol.* 63, 311–334. doi:10.1146/annurev.micro.61.080706.093130

Knoll, A. H., Bambach, R. K., Canfield, D. E., and Grotzinger, J. P. (1996). Comparative earth history and late permian mass extinction. *Science* 273, 452–457. doi:10.1126/science.273.5274.452

Knoll, A. H., Bambach, R. K., Payne, J. L., Pruss, S., and Fischer, W. W. (2007). Paleophysiology and end-Permian mass extinction. *Earth Planet Sci. Lett.* 256, 295–313. doi:10.1016/j.epsl.2007.02.018

Korte, C., and Kozur, H. W. (2010). Carbon-isotope stratigraphy across the Permian-Triassic boundary: a review. *J. Asian Earth Sci.* 39, 215–235. doi:10.1016/j.jseaes.2010.01.005

Korte, C., Kozur, H. W., and Mohtat-Aghai, P. (2004). Dzhulfian to lowermost Triassic $\delta^{13}C$ record at the Permian/Triassic boundary section at Shahreza, Central Iran. *Hallesch. Jahr. Geowissensch.* 18, 73–78.

Korte, C., Veizer, J., Leythaeuser, D., Below, R., and Schwark, L. (2001). Evolution of Permian and Lower Triassic $\delta^{13}C$ in marine and terrigenous organic material. *Terra Nostra* 2001(4), 30–34.

Krull, E. S., Lehrmann, D. J., Druke, D., Kessel, B., Yu, Y. Y., and Li, R. X. (2004). Stable carbon isotope stratigraphy across the Permian–Triassic boundary in shallow marine carbonate platforms, Nanpanjiang Basin, south China. *Palaeogeogr. Palaeoclimatol. Palaeoecol.* 204, 297–315. doi:10.1016/S0031-0182(03)00732-6

Krull, E. S., Retallack, G. J., Campbell, H. J., and Lyon, G. L. (2000a). $\delta^{13}C_{org}$ chemostratigraphy of the Permian–Triassic boundary in the Maitai Group, New Zealand: evidence for high-latitudinal methane release. *New Zealand J. Geol. Geophys.* 43, 21–32. doi:10.1080/00288306.2000.9514868

Krull, E. S., Retallack, G. J., Campbell, H. J., and Lyon, G. L. (2000b). δ13C depth profiles from paleosols across the Permian–Triassic boundary: evidence for methane release. *GSA Bull.* 112, 1459–1472. doi:10.1130/0016-7606(2000)112

Kump, L. R., and Arthur, M. A. (1999). Interpreting carbon-isotope excursions: carbonates and organic matter. *Chem. Geol.* 161, 181–198. doi:10.1016/S0009-2541(99)00086-8

Kump, L. R. (1991). Interpreting carbon-isotope excursion: strangelove oceans. *Geology* 19, 299–302. doi:10.1130/0091-7613(1991)019

Kump, L. R., Pavlov, A., and Arthur, M. A. (2005). Massive release of hydrogen sulfide to the surface ocean and atmosphere during intervals of oceanic anoxia. *Geology* 33, 397–400. doi:10.1130/G21295.1

Lai, X. L., Wang, W., Wignall, P. B., Bond, D. P. G., Jiang, H. S., Ali, J. R., et al. (2008). Palaeoenvironmental change during the end-Guadalupian (Permian) mass extinction in Sichuan, China. *Palaeogeogr. Palaeoclimatol. Palaeoecol.* 269, 78–93. doi:10.1016/j.palaeo.2008.08.005

Laws, E. A., Popp, B. N., Bidigare, R. R., Kennicutt, M. C., and Macko, S. A. (1995). Dependence of phytoplankton carbon isotopic composition on growth rate and $[CO_2]_{aq}$:theoretical considerations and experimental results. *Geochim. Cosmochim. Acta* 59, l l31-1138.

Le Vaillant, M., Barnes, S. J., Mungall, J. E., and Mungall, E. L. (2017). Role of degassing of the Noril'sk nickel deposits in the Permian–Triassic mass extinction event. *Proc. Natl. Acad. Sci. USA* 114, 2485–2490. doi:10.1073/pnas.1611086114

Li, R., and Jones, B. (2017). Diagenetic overprint on negative δ13C excursions across the Permian/Triassic boundary: a case study from Meishan section, China. *Palaeogeogr. Palaeoclimatol. Palaeoecol.* 299, 70–82. doi:10.1016/j.palaeo.2016.11.044

Liao, Z. W., Hu, W. X., Cao, J., Wang, X. L., Yao, S., and Wan, Y. (2016). Permian–Triassic boundary (PTB) in the Lower Yangtze Region, southeastern China: a new discovery of deep-water archive based on organic carbon isotopic and U–Pb geochronological studies. *Palaeogeogr. Palaeoclimatol. Palaeoecol.* 451, 124–139. doi:10.1016/j.palaeo.2016.03.004

Liu, X. C., Wang, W., Shen, S. Z., Gorgij, M. N., Ye, F. C., Zhang, Y. C., et al. (2013). Late Guadalupian to Lopingian (Permian) carbon and strontium isotopic chemostratigraphy in the Abadeh section, central Iran. *Gondwana Res.* 24, 222–232. doi:10.1016/j.gr.2012.10.012

Luo, G. M., Algeo, T. J., Huang, J. H., Zhou, W. F., Wang, Y. B., Yang, H., et al. (2014). Vertical $\delta^{13}C_{org}$ gradients record changes in planktonic microbial community composition during the end-Permian mass extinction. *Palaeogeogr. Palaeoclimatol. Palaeoecol.* 396, 119–131. doi:10.1016/j.palaeo.2014.01.006

Luo, G. M., Kump, L. R., Wang, Y. B., Tong, J., Arthur, M. A., Yang, H., et al. (2010). Isotopic evidence for an anomalously low oceanic sulfate concentration following end-Permian mass extinction. *Earth Planet Sci. Lett.* 300, 101–111. doi:10.1016/j.epsl.2010.09.041

Magaritz, M., Bär, R., Baud, A., and Holser, W. T. (1988). The carbon-isotope shift at the Permian/Triassic boundary in the Southern Alps is gradual. *Nature* 331, 337–339.

Magaritz, M., Krishnamurthy, R. V., and Holser, W. T. (1992). Parallel trends in organic and inorganic carbon isotopes across the Permian/Triassic boundary. *Am. J. Sci.* 292, 727–739. doi:10.2475/ajs.292.10.727

Mii, H. S., Grossman, E. L., and Yancey, T. E. (1997). Stable carbon and oxygen isotope shifts in Permian seas of West Spitsbergen – global change or diagenetic artifact? *Geology* 25, 227–230. doi:10.1130/0091-7613(1997)025<0227:SCAOIS>2.3.CO;2

Morante, R.. (1996). Permian and Early Triassic isotopic records of carbon and strontium in Australia and a scenario of events about the Permian-Triassic boundary. *Hist. Biol.* 11, 289–310. doi:10.1080/10292389609380546

Musashi, M., Isozaki, Y., Koike, T., and Kreulen, R. (2001). Stable carbon isotope signature in mid-Panthalassa shallow-water carbonates across the Permo-Triassic boundary: evidence for ^{13}C-depleted superocean. *Earth Planet Sci. Lett.* 191, 9–20. doi:10.1016/S0012-821X(01)00398-3

Muttoni, G., Gaetani, M., Kent, D. V., Sciunnach, D., Angiolini, L., Berra, F., et al. (2009). Opening of the neo-tethys ocean and the Pangea B to Pangea A transformation during the permian. *GeoArabia* 14, 17–48.

Nabbefeld, B., Grice, K., Schimmelmann, A., Sauer, P. E., Böttcher, M. E., and Twitchett, R. (2010). Significance of $\delta D_{kerogen}$, $\delta^{13}C_{kerogen}$ and $\delta^{34}S_{pyrite}$ from several Permian/Triassic (P/Tr) sections. *Earth Planet Sci. Lett.* 295, 21–29. doi:10.1016/j.epsl.2010.03.015

Nauta, A., Heijmans, M., Blok, D., Limpens, J., Elberling, B., Gallagher, A., et al. (2015). Permafrost collapse after shrub removal shifts tundra ecosystem to a methane source. *Nat. Clim. Change* 5, 67–70. doi:10.1038/nclimate2446

Nazaries, L., Murrell, J. C., Millard, P., Baggs, L., and Singh, B. K. (2013). Methane, microbes and models: fundamental understanding of the soil methane cycle for future predictions. *Environ. Microbiol.* 15, 2395–2417. doi:10.1111/1462-2920.12149

Oh, Y., Zhuang, Q., Liu, L., Welp, L. R., Lau, M. C. Y., Onstott, T. C., et al. (2020). Reduced net methane emissions due to microbial methane oxidation in a warmer Arctic. *Nat. Clim. Chang.* 10, 317–321. doi:10.1038/s41558-020-0734-z

Payne, J. L., and Clapham, M. E. (2012). End-Permian mass extinction in the oceans: an ancient analog for the twenty-first century? *Ann. Rev. Earth Planet. Sci.* 40, 89–111. doi:10.1146/annurev-earth-042711-105329

Payne, J. L., Lehrmann, D. J., Follett, D., Seibel, M., Kump, L. R., Riccardi, A., et al. (2007). Erosional truncation of uppermost Permian shallow-marine carbonates and implications for Permian-Triassic boundary events. *GSA Bull.* 119, 771–784. doi:10.1130/B26091.1

Polozov, A. G., Svensen, H. H., Planke, S., Grishina, S. N., Fristad, K. E., and Jerram, D. A. (2016). The basalt pipes of the Tunguska Basin (Siberia, Russia): high temperature processes and volatile degassing into the end-Permian atmosphere. *Palaeogeogr. Palaeoclimatol. Palaeoecol.* 441, 51–64. doi:10.1016/j.palaeo.2015.06.035

Popp, B. N., Takigiku, R., Hayes, J. M., Louda, J. W., and Baker, E. W. (1989). The post-Paleozoic Chronology and Mechanism of ^{13}C Depletion in primary marine organic matter. *Am. J. Sci.* 289, 436–454.

Preuss, A., Schauder, R., Fuchs, G., and Stichler, W. (1989). Carbon isotope fractionation by autotrophic bacteria with three different CO_2 fixation pathways. *Z. Naturforsch*. 44c, 397–402.

Racki, G. (2020). "Big 5 mass extinctions." in *Encyclopedia of geology*. 2nd Edition, Editors S. Elias and D. D. Alderton, (Newyork, United States: Elsevier), pp. 1–14. doi:10.1016/B978-0-12-409548-9.12028.7

Rampino, M. R., and Caldeira, K. (2005). Major perturbation of ocean chemistry and a 'Strangelove Ocean' after the end-Permian mass extinction. *Terra. Nova* 17, 554–559. doi:10.1111/j.1365-3121.2005.00648.x

Rampino, M. R., Rodriguez, S., Baransky, E., and Cai, Y. (2017). Global nickel anomaly links Siberian Traps eruptions and the latest Permian mass extinction. *Sci. Rep*. 7, 12416. doi:10.1038/s41598-017-12759-9

Rau, G. H., Riebesell, U., and Wolf-Gladrow, D. (1997). $CO_{2,aq}$-dependent photosynthetic ^{13}C fractionation in the ocean: A model versus measurements. *Global Biogeochem. Cycles* 11, 267–278. doi:10.1029/97GB00328

Rau, G. H., Takahaski, T., Des Marais, D. J., Repeta, D. J., and Martin, J. H. (1992). The relationship between $\delta^{13}C$ of organic matter and $^{[}CO_{2,aq}{}^{]}$ in ocean surface water: data from a JGOFS site in the northeast Atlantic Ocean and a model. *Geochim. Cosmochim. Acta* 56, 1413–1419. doi:10.1016/0016-7037(92)90073-R

Reeburgh, W. S. (2007). Oceanic methane biogeochemistry. *Chem. Rev*. 107, 486–513. doi:10.1021/cr050362v

Reichow, M. K., Pringle, M. S., Al'Mukhamedov, A. I., Allen, M. B., Andreichev, V. L., Buslov, M. M., et al. (2009). The timing and extent of the eruption of the Siberian Traps large igneous province: implications for the end-Permian environmental crisis. *Earth Planet Sci. Lett*. 277, 9–20. doi:10.1016/j.epsl.2008.09.030

Renne, P. R., and Basu, A. R. (1991). Rapid eruption of the Siberian traps flood basalts at the Permian-Triassic boundary. *Science* 253, 176–179. doi:10.1126/science.253.5016.176

Renne, P. R., Zichao, Z., Richards, M. A., Black, M., and Basu, A. R. (1995). Synchrony and causal relations between Permian-Triassic boundary crises and Siberian flood volcanism. *Science* 269, 1413–1416. doi:10.1126/science.269.5229.1413

Retallack, G. J. (2005). Earliest triassic claystone breccias and soil-erosion crisis. *J. Sed. Res*. 75, 679–695. doi:10.2110/jsr.2005.055

Retallack, G. J., and Jahren, A. H. (2008). Methane release from igneous intrusion of coal during Late Permian extinction events. *J. Geol*. 116, 1–20. doi:10.1086/524120

Retallack, G. J., Jahren, A. H., Sheldon, N. D., Chakrabarti, R., Metzger, C. A., and Smith, R. M. H. (2005). The permian–triassic boundary in Antarctica. *Antarctic Sci*. 17, 241–258. doi:10.1017/S0954102005002658

Retallack, G. J., and Krull, E. S. (2006). "Carbon isotopic evidence for terminal-Permian methane outbursts and their role in extinctions of animals, plants, coral reefs, and peat swamps." in *Wetlands through time*. Editors S. F. Greb and W. A. DiMichele, (Boulder: Geol. Soc. Am. Spec. Pap.) 399, 249–268. doi:10.1130/2006.2399(12

Retallack, G. J., Veevers, J. J., and Morante, R. (1996). Global coal gap between Permian–Triassic extinction and Middle Triassic recovery of peat-forming plants. *GSA Bull*. 108, 195–207. doi:10.1130/0016-7606(1996)108<0195:GCGBPT>2.3.CO;2

Riccardi, A., Kump, L. R., Arthur, M. A., and D'Hondt, S. (2007). Carbon isotopic evidence for chemocline upward excursions during the end-Permian event. *Palaeogeogr. Palaeoclimatol. Palaeoecol*. 248, 73–81. doi:10.1016/j.palaeo.2006.11.010

Richoz, S. (2006). Stratigraphie et variations isotopiques du carbone dans le Permien supérieur et le Trias inférieur de la Néotéthys (Turquie, Oman et Iran). *Mem. Géol*. 46, 251.

Rothman, D. H., Fournier, G. P., French, K. L., Alm, E. J., Boyle, E. A., Cao, C. Q., et al. (2014). Methanogenic burst in the end-Permian carbon cycle. *Proc. Natl. Acad. Sci. USA* 111, 5462–5467. doi:10.1073/pnas.1318106111

Ryskin, G. (2003). Methane-driven oceanic eruptions and mass extinctions. *Geology* 31, 741–744. doi:10.1130/G19518.1

Saitoh, M., Isozaki, Y., Ueno, Y., Yoshida, N., Yao, J. X., and Ji, Z. S. (2013b). Middle-Upper Permian carbon isotope stratigraphy at Chaotian, South China: pre-extinction multiple upwelling of oxygen-depleted water onto continental shelf. *J. Asian Earth Sci*. 67-68, 51–62. doi:10.1016/j.jseaes.2013.02.009

Saitoh, M., Isozaki, Y., Yao, J. X., Ji, Z. S., Ueno, Y., and Yoshida, N. (2013a). The appearance of an oxygen-depleted condition on the Capitanian disphotic slope/basin in South China: middle-Upper Permian stratigraphy at Chaotian in northern Sichuan. *Glob. Planet. Change* 105, 180–192. doi:10.1016/j.gloplacha.2012.01.002

Saitoh, M., Ueno, Y., Isozaki, Y., Nishizawa, M., Shozugawa, K., Kawamura, T., et al. (2014b). Isotopic evidence for water-column denitrification and sulfate reduction at the end-Guadalupian (Middle Permian). *Glob. Planet. Change* 123, 110–120. doi:10.1016/j.jseaes.2014.06.026

Saitoh, M., Ueno, Y., Isozaki, Y., Shibuya, T., Yao, J. X., Ji, Z. S., et al. (2015). Authigenic carbonate precipitation at the end-Guadalupian (Middle Permian) in China: implications for the carbon cycle in ancient anoxic oceans. *Prog. Earth Planet. Sci*. 2:41. doi:10.1186/s40645-015-0073-2

Saitoh, M., Ueno, Y., Matsu'ura, F., Kawamura, T., Isozaki, Y., Yao, J. X., et al. (2017). Multiple sulfur isotope records at the end-Guadalupian (Permian) at Chaotian, China: implications for a role of bioturbation in the Phanerozoic sulfur cycle. *J. Asian Earth Sci*. 135, 70–79. doi:10.1016/j.jseaes.2016.12.009

Saitoh, M., Ueno, Y., Nishizawa, M., Isozaki, Y., Takai, K., Yao, J. X., et al. (2014a). Nitrogen isotope chemostratigraphy across the permian-triassic boundary at chaotian, sichuan, south China. *J. Asian Earth Sci*. 93, 113–128. doi:10.1016/j.gloplacha.2014.10.014

Saltzman, M. R., and Sedlacek, A. R. C. (2013). Chemostratigraphy indicates a relatively complete Late Permian to Early Triassic sequence in the western United States. *Geology* 41, 399–402. doi:10.1130/G33906.1

Sarkar, A., Yoshioka, H., Ebihara, M., and Naraoka, H. (2003). Geochemical and organic carbon isotope studies across the continental Permo–Triassic boundary of Raniganj Basin, eastern India. *Palaeogeogr. Palaeoclimatol. Palaeoecol*. 191, 1–14. doi:10.1016/S0031-0182(02)00636-3

Saunders, A., and Reichow, M. (2009). The Siberian Traps and the End-Permian mass extinction: a critical review. *Chin. Sci. Bull*. 54, 20–37. doi:10.1007/s11434-008-0543-7

Schidlowski, M., Hayes, J. M., and Kaplan, I. R. (1983). "Isotopic inferences of ancient biochemistries: carbon, sulfur, hydrogen, and nitrogen." in *Earth's earliest biosphere*. Editor J. W. Schopf (Princeton, NJ: Princeton University Press), 149–186.

Schneebeli-Hermann, E. (2012). Extinguishing a permian world. *Geology* 40, 287–288. doi:10.1130/focus032012.1

Schneebeli-Hermann, E., Kürschner, W. M., Hochuli, P. A., Ware, D., Weissert, H., Bernasconi, S. M., et al. (2013). Evidence for atmospheric carbon injection during the end-Permian extinction. *Geology*. 41, 579–582. doi:10.1130/G34047.1

Schobben, M., Stebbins, A., Algeo, T. J., Strauss, H., Leda, L., Haas, J., et al. (2017). Volatile earliest Triassic sulfur cycle: a consequence of persistent low seawater sulfate concentrations and a high sulfur cycle turnover rate? *Palaeogeogr. Palaeoclimatol. Palaeoecol*. 486, 74–85. doi:10.1016/j.palaeo.2017.02.025

Schobben, M., Stebbins, A., Ghaderi, A., Strauss, H., Korn, D., and Korte, C. (2015). Flourishing ocean drives the end-Permian marine mass extinction. *Proc. Natl. Acad. Sci. USA*. 112, 10298–10303. doi:10.1073/pnas.1503755112

Schobben, M., Ullmann, C. V., Leda, L., Korn, D., Struck, U., Reimold, W. U., et al. (2016). Discerning primary versus diagenetic signals in carbonate carbon and oxygen isotope records: an example from the Permian–Triassic boundary of Iran. *Chem. Geol*. 422, 94–107. doi:10.1016/j.chemgeo.2015.12.013

Scholze, F., Wang, X., Kirscher, U., Kraft, J., Schneider, J. W., Götz, A. E., et al. (2017). A multistratigraphic approach to pinpoint the Permian-Triassic boundary in continental deposits: the Zechstein–Lower Buntsandstein transition in Germany. *Global Planet. Change*. 152, 129–151. doi:10.1016/j.gloplacha.2017.03.004

Sephton, M. A., Looy, C. V., Brinkhuis, H., Wignall, P. B., de Leeuw, J. W., and Visscher, H. (2005). Catastrophic soil erosion during the end-Permian biotic crisis. *Geology*. 33, 941–944. doi:10.1130/G21784.1

Sephton, M. A., Looy, C. V., Veefkind, R. J., Brinkhuis, H., de Leeuw, J. W., and Visscher, H. (2002). "Synchronous record of $\delta^{13}C$ shifts in the oceans and atmosphere at the end of the Permian." in *Catastrophic events and mass extinctions: impacts and beyond*., Editors C. Koeberl and K. G. MacLeod (Boulder: Geol. Soc. Am. Spec. Pap.) Vol. 356, pp. 455–462.

Shao, L., Zhang, P. F., Dou, J. W., and Shen, S. Z. (2000). Carbon isotope compositions of the Late Permian carbonate rocks in southern China: their variations between the Wujiaping and Changxing formations. *Palaeogeogr. Palaeoclimatol. Palaeoecol*. 161, 179–192. doi:10.1016/S0031-0182(00)00122-X

Shen, J., Algeo, T. J., Hu, Q., Zhang, N., Zhou, L., Xia, W. C., et al. (2012). Negative C-isotope excursions at the Permian-Triassic boundary linked to volcanism. *Geology* 40, 963–966. doi:10.1130/G33329.1

Shen, S. Z., Cao, C. Q., Zhang, H., Bowring, S. A., Henderson, C. M., Payne, J. L., et al. (2013). High- resolution $\delta^{13}C_{carb}$ chemostratigraphy from latest Guadalupian through earliest Triassic in South China and Iran. *Earth Planet Sci. Lett*. 375, 156–165. doi:10.1016/j.epsl.2013.05.020

Shen, S. Z., Crowley, J. L., Wang, Y., Bowring, S. A., Erwin, D. H., Sadler, P. M., et al. (2011a). Calibrating the end-Permian mass extinction. *Science* 334, 1367–1372. doi:10.1126/science.1213454

Shen, W. J., Sun, Y. G., Lin, Y. T., Liu, D. H., and Chai, P. X. (2011b). Evidence for wildfire in the Meishan section and implications for Permian–Triassic events. *Geochim. Cosmochim. Acta* 75, 1992–2006. doi:10.1016/j.gca.2011.01.027

Shen, Y., Farquhar, J., Zhang, H., Masterson, A., Zhang, T. G., and Wing, B. A. (2011c). Multiple S-isotopic evidence for episodic shoaling of anoxic water during Late Permian mass extinction. *Nat. Commun*. 2, 210. doi:10.1038/ncomms1217

Siegert, S., Kraus, S. H., Mette, W., Struck, U., and Korte, C. (2011). Organic carbon isotope values from the Late Permian Seis/Siusi succession (Dolomites, Italy): implications for palaeoenvironmental changes. *Fossil Record* 14, 207–217. doi:10.1002/mmng.201100008

Singh, B. K., Bardgett, R. D., Smith, P., and Reay, D. S. (2010). Microorganisms and climate change: terrestrial feedbacks and mitigation options. *Nat. Rev. Microbiol*. 8, 779–790. doi:10.1038/nrmicro2439

Song, H. J., Tong, J. N., Xiong, Y. L., Sun, D. Y., Tian, L., and Song, H. Y. (2012a). The large increase of $^{13}C_{carb}$-depth gradient and the end-Permian mass extinction. *Sci. Chin. Earth Sci*. 55, 1101–1109. doi:10.1007/s11430-012-4416-1

Song, H. J., Wignall, P. B., Tong, J., Bond, D. P. G., Song, H. Y., Lai, X. L., et al. (2012b). Geochemical evidence from bio-apatite for multiple oceanic anoxic events during Permian–Triassic transition and the link with end-Permian extinction and recovery. *Earth Planet Sci. Lett*. 353-354, 12–21. doi:10.1016/j.epsl.2012.07.005

Stanley, S. M.. (2016). Estimates of the magnitudes of major marine mass extinctions in earth history. *Proc. Natl. Acad. Sci. USA* 113, E6325–E6334. doi:10.1073/pnas.1613094113

Stebbins, A., Algeo, T. J., Olsen, C., Sano, H., Rowe, H., and Hannigan, R. (2019). Sulfur-isotope evidence for recovery of seawater sulfate concentrations from a PTB minimum by the Smithian-Spathian transition. *Earth-Sci. Rev*. 195, 83–95. doi:10.1016/j.earscirev.2018.08.010

Sun, Y., Joachimski, M. M., Wignall, P. B., Yan, C., Chen, Y., Jiang, H., et al. (2012). Lethally hot temperatures during the Early Triassic greenhouse. *Science* 338, 366–370. doi:10.1126/science.1224126

Svensen, H., Planke, S., Polozov, A. G., Schmidbauer, N., Corfu, F., Podladchikov, Y. Y., et al. (2009). Siberian gas venting and the end-Permian environmental crisis. *Earth Planet Sci. Lett*. 277, 490–500. doi:10.1016/j.epsl.2008.11.015

Takahashi, S., Kaiho, K., Oba, M., and Kakegawa, T. (2010). A smooth negative shift of organic carbon isotope ratios at an end-Permian mass extinction horizon in central pelagic Panthalassa. *Palaeogeogr. Palaeoclimatol. Palaeoecol*. 292, 532–539. doi:10.1016/j.palaeo.2010.04.025

Tohver, E., Cawood, P. A., Riccomini, C., Lana, C., and Trindade, R. I. F. (2013). Shaking a methane fizz: seismicity from the Araguainha impact event and the Permian–Triassic global carbon isotope record. *Palaeogeogr. Palaeoclimatol. Palaeoecol*. 387, 66–75. doi:10.1016/j.palaeo.2013.07.010

Twitchett, R. J., Looy, C. V., Morante, R., Visscher, H., and Wignall, P. B. (2001). Rapid and synchronous collapse of marine and terrestrial ecosystems during the end- Permian biotic crisis. *Geology* 29, 351–354. doi:10.1130/0091-7613(2001)029

Vajda, V., McLoughlin, S., Mays, C., Frank, T. D., Fielding, C. R., Tevyaw, A., et al. (2020). End-Permian (252 Mya) deforestation, wildfires and flooding–An ancient biotic crisis with lessons for the present. *Earth Planet Sci. Lett*. 529, 115875. doi:10.1016/j.epsl.2019.115875

van Breugel, Y., Schouten, S., Paetzel, M., Ossebaar, J., and Sinninghe Damsté, J. S. (2005). Reconstruction of $\delta^{13}C$ of chemocline CO2 (aq) in past oceans and lakes using the $\delta^{13}C$ of fossil isorenieratene. *Earth Planet Sci. Lett*. 235, 421–434. doi:10.1016/j.epsl.2005.04.017

van Groenigen, K., Osenberg, C., and Hungate, B. (2011). Increased soil emissions of potent greenhouse gases under increased atmospheric CO_2. *Nature* 475, 214–216. doi:10.1038/nature10176

Wang, Y., and Jin, Y. (2000). Permian palaeogeographic evolution of the jiangnan basin, south China. *Palaeogeogr. Palaeoclimatol. Palaeoecol*. 160, 35–44. doi:10.1016/S0031-0182(00)00043-2

Ward, P. D., Botha, J., Buick, R., De Kock, M. O., Erwin, D. H., Garrison, G. H., et al. (2005). Abrupt and gradual extinction among Late Permian land vertebrates in the Karoo Basin, South Africa. *Science* 307, 709–714. doi:10.1126/science.1107068

Ward, P. D., Montgomery, D. R., and Smith, R. (2000). Altered river morphology in South Africa related to the Permian–Triassic extinction. *Science* 289, 1740–1743. doi:10.1126/science.289.5485.1740

Wei, H., Yu, H., Wang, J. G., Qiu, Z., Xiang, L., and Shi, G. (2015). Carbon isotopic shift and its cause at the Wuchiapingian–Changhsingian boundary in the Upper Permian at the Zhaojiaba section, South China: evidences from multiple geochemical proxies. *J. Asian Earth Sci*. 105, 270–285. doi:10.1016/j.jseaes.2015.01.011

Wignall, P. B., and Hallam, A. (1992). Anoxia as a cause of the Permian/Triassic mass extinction: facies evidence from northern Italy and the western United States. *Palaeogeogr. Palaeoclimatol. Palaeoecol*. 93, 21–46. doi:10.1016/0031-0182(92)90182-5

Wignall, P. B. (2001). Large igneous provinces and mass extinctions. *Earth-Sci. Rev*. 53, 1–33. doi:10.1016/S0012-8252(00)00037-4

Wignall, P. B., Morante, R., and Newton, R. (1998). The Permo–Triassic transition in Spitsbergen: $\delta^{13}C_{org}$ chemostratigraphy, Fe and S geochemistry, facies, fauna and trace fossils. *Geol. Mag*. 135, 47–62. doi:10.1017/S0016756897008121

Wignall, P. B., and Twitchett (1996). Oceanic anoxia and end Permian mass extinction. *Science* 272, 1155–1158. doi:10.1126/science.272.5265.1155

Xie, S. C., Pancost, R. D., Huang, J. H., Wignall, P. B., Yu, J. X., Tang, X. Y., et al. (2007). Changes in the global carbon cycle occurred as two episodes during the Permian–Triassic crisis. *Geology* 35, 1083–1086. doi:10.1130/G24224A.1

Xu, D. Y., Ma, S. L., Chai, Z. F., Mao, X. Y., Sun, Y. Y., Zhang, Q. W., et al. (1985). Abundance variation of iridium and trace elements at the Permian/Triassic boundary at Shangsi in China. *Nature* 314, 154–156.

Yang, B., Li, H. X., Wignall, P. B., Jiang, H. S., Niu, Z. J., Ye, Q., et al. (2019). Latest wuchiapingian to earliest triassic conodont zones and δ13Ccarb isotope excursions from deep-water sections in western Hubei province, south China. *J. Earth Sci*. 30, 1059–1074. doi:10.1007/s12583-019-1018-2

Yang, Z. Y., Yin, H. F., Wu, S. B., Yang, F. Q., Ding, M. H., and Xu, G. R. (1987). Permian-triassic boundary. Stratigraphy and faunas of South China. Ministry of geology and mineral resources. *Geol. Mem. Ser*. 26, 1–379 (in Chinese with English abstract).

Yin, H. F., Jiang, H. S., Xia, W. C., Feng, Q. L., Zhang, N., and Shen, J. (2014). The end-Permian regression in South China and its implication on mass extinction. *Earth-Sci. Rev*. 137, 19–33. doi:10.1016/j.earscirev.2013.06.003

Yuan, D. X., Chen, J., Zhang, Y. C., Zheng, Q. F., and Shen, S. Z. (2015). Changhsingian conodont succession and the end-Permian mass extinction event at the Daijiagou section in Chongqing, Southwest China. *J. Asian Earth Sci*. 105, 234–251. doi:10.1016/j.jseaes.2015.04.002

Yvon-Durocher, G., Allen, A., Bastviken, D., Conrad, R., Gudasz, C., St-Pierre, A., et al. (2014). Methane fluxes show consistent temperature dependence across microbial to ecosystem scales. *Nature* 507, 488–491. doi:10.1038/nature13164

Zhang, G. J., Zhang, X. L., Hu, D. P., Li, D. D., Algeo, T. J., Farquhar, J., et al. (2017). Redox chemistry changes in the Panthalassic ocean linked to the end-Permian mass extinction and delayed Early Triassic biotic recovery. *Proc. Natl. Acad. Sci. USA* 114, 1806–1810. doi:10.1073/pnas.1610931114

Zhao, J. K., Liang, X. L., and Zheng, Z. G. (1978). Late permian cephalopods of South China. *Palaeontol. Sinica, N.S.* 12, 1–194 (in Chinese with English abstract).

Zhao, J. K., Sheng, J. Z., Yao, Z. Q., Liang, X. L., Chen, C. Z., Rui, L., et al. (1981). The changhsingian and permian-triassic boundary of South China. *Bull. Nanjing Inst. Geol. Paleontol. Acad. Sinica* 2, 1–112 (in Chinese).

Zhou, W. F., Algeo, T. J., Ruan, X. Y., Luo, G. M., Chen, Z. Q., and Xie, S. C. (2017). Expansion of photic-zone euxinia during the Permian–Triassic biotic crisis and its causes: microbial biomarker records. *Palaeogeogr. Palaeoclimatol. Palaeoecol*. 474, 140–151. doi:10.1016/j.palaeo.2016.06.027

Zhu, T. X., Huang, Z. Y., and Hui, L. (1999). *The geology of late permian period biohermal facies in upper yangtze tableland*. Beijing, China: Geol. Pub. House, (in Chinese).

Zuchuat, V., Sleveland, A. R. N., Twitchett, R. J., Svensen, H. H., Turner, H., Augland, L. E., et al. (2020). A new high-resolution stratigraphic and palaeoenvironmental record spanning the End-Permian Mass Extinction and its aftermath in central Spitsbergen. *Svalbard. Palaeogeogr. Palaeoclimatol. Palaeoecol*. 554, 109732. doi:10.1016/j.palaeo.2020.109732

Conflict of Interest: The authors declare that the research was conducted in the absence of any commercial or financial relationships that could be construed as a potential conflict of interest.